Parasitic worm product ES-62 promotes healthspan and lifespan in a mouse model of obesity-induced ageing

Running Title: ES-62 promotes healthspan

Jenny Crowe[a*], Felicity E. Lumb[b*], James Doonan[b], Ana Tarafdar[a], Miguel A Pineda[a], Paul A. Hoskisson[b], Simon A. Babayan[c], Colin Selman[c], William Harnett[b†] and Margaret M. Harnett[a†]

[a]Institute of Infection, Immunity and Inflammation, University of Glasgow, Glasgow G12 8TA, UK

[a]Strathclyde Institute of Pharmacy and Biomedical Sciences, University of Strathclyde, Glasgow, G4 0RE, UK

[c]Glasgow Ageing Research Network (GARNER), Institute of Biodiversity, Animal Health and Comparative Medicine, University of Glasgow, Glasgow, G12 8QQ, UK

* Joint first authors

†Corresponding authors:

Margaret Harnett, Institute of Infection, Immunity and Inflammation, College of Medical, Veterinary and Life Sciences, University of Glasgow, Glasgow G12 8TA, UK; Phone – 0044-141-330-8413; e.mail – Margaret.Harnett@glasgow.ac.uk

William Harnett, Strathclyde Institute of Pharmacy and Biomedical Sciences, 161 Cathedral Street, University of Strathclyde, Glasgow G4 0RE, UK; Phone – 0044-141-548-3715; FAX: 0044-141-552-2562; e.mail: w.harnett@strath.ac.uk

Abstract

The recent increase in human lifespan but not healthspan has led to the search for novel interventions that improve late-life health. Development of ageing-associated co-morbidities is associated with chronic low grade inflammation and this is enhanced by the high calorie Western diet (HCD). Here we focus on ES-62, an immunomodulator secreted by the parasitic worm *Acanthocheilonema viteae* that we have previously shown to have potent anti-inflammatory properties. ES-62 was tested in a C57BL/6J mouse model of HCD-accelerated ageing and found to ameliorate pathophysiological, inflammatory and metabolic parameters, when administered at just 1 μg/week. Strikingly, the worm product also significantly increased the median survival time but only in male HCD-mice. Consistent with this, ES-62 showed different protective effects in male versus female mice and in combination with a machine learning approach, this has provided indications of key parameters that may promote both healthspan and lifespan, and that thus represent therapeutic targets.

Introduction

Adoption of the modern Western diet (high fat and sugar) has significantly contributed to a global pandemic in metabolic syndrome, obesity, type-2 diabetes (T2D) and cardiovascular disease (CVD); ageing-associated conditions that impact on both wellbeing (healthspan) and lifespan[1,2]. This increasing major public health concern reflects, at least in part, that such a high calorie diet (HCD) disrupts the gut microbiome, with the consequent intestinal inflammation and loss of barrier integrity driving chronic systemic inflammation that appears to dysregulate immunometabolic pathways, accelerating the ageing process and reducing lifespan[1,3-7]. Interestingly,

epidemiological data suggest that Western diet-associated diseases are rising fastest in in the developing world [2,8], regions where parasitic worms (helminths) and other infectious agents are being rapidly eradicated[9]. Helminths promote their survival by releasing excretory-secretory products (ES) that, by dampening inflammation and promoting tissue repair, act to prevent worm expulsion but also limit host pathology[10]. Thus, the relatively rapid eradication of these parasites appears to have resulted in host hyper-active immune systems, characterised by chronic low-grade inflammation that may (further) contribute to development of obesity and associated metabolic syndrome co-morbidities, as well as allergic and autoimmune inflammatory disorders, in developing and urbanised countries[10]. Whilst this has questioned the wisdom of current mass parasite eradication programs, it has emphasised the potential of utilising worm infections or ES to treat a wide range of non-communicable diseases that are characterised by chronic TLR/MyD88-mediated inflammation[11 12,13]. Supporting this, we have shown that a single, defined ES product, ES-62, a protein containing phosphorylcholine groups attached to *N*-type glycans, can suppress pathology in mouse models of allergic and autoimmune inflammatory diseases[9,10,14-16]. ES-62 achieves this by normalising aberrant MyD88 signalling to homeostatically restore immunoregulation, irrespective of the inflammatory phenotype[9]. MyD88 is increasingly recognized as a key innate receptor transducer and integrator of dysregulated inflammatory and metabolic pathways [11,17-19]. Indeed, adoption of a HCD induces reprogramming of innate immune responses resulting in chronic TLR4/MyD88 signalling[20], which has been shown to play critical roles in promoting diet-induced myelopoiesis and the generation of M1-like (CD11c+) macrophages and consequent inflammation in adipose tissue[21], as well as in glucose intolerance, β-cell failure and inflammation of metabolic tissues (pancreas

and liver). Furthermore, critically, these HCD-TLR4/MyD88-induced effects are exacerbated by ageing[22]. Thus, based on ES-62's targeting of MyD88 and demonstrable ability to protect against diseases associated with aberrant inflammation, we investigated whether it could shield against HCD-associated decreases in healthspan and lifespan in C57BL/6J mice. Our approach of combining longitudinal (survival) and cross-sectional (intervention) studies has revealed dynamic and differential diet-, gender-, age- and ES-62 (treatment)-associated immunological and metabolic profiles of healthspan. However, excitingly, ES-62 (differentially) improves healthspan in both male and female HCD-fed mice and substantially extends median lifespan of male HCD-fed mice.

Results & Discussion

ES-62 extends lifespan in male C57BL/6 mice fed a high calorie diet (HCD)

We investigated whether ES-62 could modulate the lifespan of a mixed gender cohort of HCD-fed C57BL/6 mice. Although overall the effects of ES-62 treatment did not achieve statistical significance (median survival; PBS, 641 days; ES-62, 661 days; Fig. 1a), consistent with interventions that impact on health- and lifespan often exhibiting significant sexual dimorphism[23-25], significant gender differences were evident (Fig. 1b-e; Supplementary Table 1). Thus, ES-62 substantially extended the median lifespan of male, but not female, HCD-mice (from 629 to 703 days [>10%], *$p<0.05$ at day 660). Whilst female HCD-PBS-fed mice had a slightly higher median survival span than their male counterparts (653 v 629 days), this did not reach statistical significance and there were no significant differences amongst male HCD-PBS and female HCD-PBS or HCD-ES-62 mice (Fig. 1a-e; Supplementary Table 1).

Previous studies in mice fed a normal diet (chow) showed that body weight of male (mean, 40 g) and female (mean, 34 g) mice plateaus around 420 days of age before declining from about day-600 and -720, respectively, with low body mass (BM), particularly in early life, being associated with longevity in genetically heterogeneous mice[26]. By contrast, the mean peak BM of our male HCD-fed mice was only slightly higher (although statistically significant) than that of their female counterparts (56.20 ± 0.93 g, n=23 versus 53.19 ± 1.32 g, n=24, $p<0.05$) and whilst the male HCD-PBS mice reached their maximum body weight at around the same age as chow-fed mice, female HCD-fed mice did not achieve this until they were significantly older (431.8 ± 15.22 versus 513 ±11.14 days, $p<0.001$; Fig. 1f). Moreover, although BM declined sharply after reaching their maximal levels in male HCD (PBS and ES-62)-mice, female HCD-PBS mice maintained a relatively stable body weight until death: however, ES-62-treated female HCD mice exhibited a similar decline in weight to that of the aged male HCD cohorts (Fig. 1f). Notably, the extension of life-span in male HCD-fed mice did not reflect prevention of increased body mass (BM) as ES-62 did not significantly modulate either peak BM (57.22 ± 1.10 g male and 50.77 ± 1.17 g female, respectively) or the BM of male HCD mice over their life-course (Fig. 1f). Food intake was not altered in either male or female HCD-fed mice (Fig. 1g).

Whilst the extent of the change in BM observed over the life course negatively correlated with longevity in the male HCD-PBS mice (r=-0.5593, **<0.01 n=22 xy pairs), this was not the case for the HCD-ES-62 (r=-0.2237, ns n=20 xy pairs) or female HCD (r=0.1009, ns n=22 xy pairs) cohorts. However, and perhaps consistent with ES-62-treated female HCD-fed mice exhibiting a similar decline in BM to that of the ageing male HCD-fed mice, the extent of change in BM also negatively

correlated with lifespan in the female HCD-ES-62 (r=-0.4479, *<0.05, n=23 xy pairs) group (Supplementary Fig.1a & b). However, there was no correlation between the peak BM achieved by individual mice and their longevity in any of the cohorts (Supplementary Fig. 1c & d), the latter result mirroring findings that maximum BM is also not a good predictor of longevity in mice fed a normal diet[26]. Moreover, whilst a significant association (peaking about 150 days of age) between low BM and longevity has been reported in chow-fed mice when measured between 60-720 days of age[26], we found no such correlation for any of the HCD-fed cohorts when BM was measured at 116, 160, 340 or 500 days of age (Supplementary Figure 1e-n). Rather, perhaps critically, ES-62 appeared to protect against the loss of weight generally occurring during old age (>720-day old mice, approx >70 human years) in male, but not female, HCD-fed mice (Fig. 1f). However, there was no corresponding protection against the decline in grip strength associated with ageing (Fig. 1h) and reflecting this, there was no significant correlation between the decline from peak grip strength and longevity with any cohort (Supplementary Fig. 1o & p).

As expected given their life-long exposure to an energy rich diet, many of the mice in this lifespan study exhibited evidence of liver tumours upon post mortem irrespective of gender or treatment (Supplementary Tables 2 & 3), presumably as a consequence of the HCD-induction of insulin resistance and non-alcoholic fatty liver disease (NAFLD). We therefore addressed the impact of ES-62 on metabolic tissues and their associated dysregulated metabolic responses in a series of cross-sectional studies (at d160, d340 and d500) on male and female HCD-fed mice, with reference to young (day 56) and aged-matched normal chow-fed control cohorts.

Modulation of the impact of HCD on BM and metabolic tissues by ES-62

Firstly, the mice in the cross-sectional cohorts exhibited very similar kinetics of BM gain over their respective time courses, compared to those in the longevity cohorts (Supplementary Fig. 2). Indeed, analysis of their mean BM values confirmed that ES-62 had no significant effect on HCD-induced obesity, with HCD-male and -female mice regardless of treatment showing substantially higher BM than their aged-matched chow control groups and male mice being, on average, significantly heavier at cull than their female counterparts (***$p<0.001$) at each of these timepoints (Fig. 1i & j). Analysis of their metabolic organs revealed that HCD-fed mice exhibit substantial increases in visceral (gonadal and retroperitoneal depots; normalised to total BM; Figs, 1k-n) fat during ageing, relative to their normal chow controls. Consistent with the loss of metabolic regulation occurring during ageing[3], mice fed a normal diet also showed pronounced increases in their levels of visceral fat, particularly in the d500 cohorts (Fig. 1k-n). By contrast, although a substantial increase was detected in the male cohort by d160, the HCD appeared to have less overall effect on liver mass in obese female mice (Fig. 1o & p). Exposure to ES-62 generally had marginal effects on metabolic organ size in HCD-fed mice, however, the livers from the male HCD-ES-62 cohort were found to be significantly smaller than those from their (PBS) control group at d500.

ES-62 protects adipocyte health in HCD-fed mice

Deeper analysis revealed that, as expected, male and female mice fed a HCD exhibited pronounced adipocyte hypertrophy in both visceral fat deposits, relative to their normal chow controls, that was evident by the day 160 timepoint (Fig. 2a-h). Significant hyperplasia of (small) adipocytes was not detected, as evidenced by the

corresponding decrease in adipocyte numbers in the tissue sections (Supplementary Fig. 3a-d). However, whilst the adipocytes in gonadal fat from either the male or female chow-fed cohorts showed marginal or no increase in size, conversely, at d500 those in retroperitoneal fat were not significantly different from their HCD-PBS counterparts, with clear increases in adipocyte size being detected by d160 in the male chow-fed cohort. Interestingly therefore, whilst ES-62 was able to reduce the hypertrophy observed in both visceral fat depots in male HCD mice, it was only able to delay the HCD-increase in adipocyte size in retroperitoneal fat and had no effect on gonadal adipocyte area in female HCD-mice. Perhaps pertinent to this, ES-62 was able to reduce expression of TripB2, a key transcription factor driving adiposity and regulating energy metabolism[27] in gonadal fat from male, but not female, HCD-fed mice at d340 (Fig. 2i & j). Indeed, male TripBr2-deficient mice show reduced pro-inflammatory cytokine production in adipose tissue and are protected against insulin resistance and obesity in an acute (12 week) model of diet-induced obesity[27]. Perhaps surprisingly therefore, the highest expression of TripBr2 was observed in the female chow d160 and d340 cohorts: however, lean human females were previously shown to exhibit higher levels of fat-associated TripBr2 expression than male subjects, these being more similar to those seen in subcutaneous fat from male obesity cohorts[27]. Moreover, in male mice, the retroperitoneal, but not gonadal, adipocytes in ES-62-treated HCD-fed mice more closely resembled the morphology of those from the chow-fed rather than PBS-HCD cohorts. Collectively, these data suggest that ES-62 may act to protect adipocyte metabolic function, but particularly in male HCD-mice.

To investigate the potential mechanisms involved, we examined the effect of ES-62

on eosinophil levels in the visceral fat depots. These cells have been proposed to maintain adipocyte health by promoting M2-like macrophages that act to preserve metabolic function and prevent adiposity and systemic insulin resistance[28,29]. Consistent with this, whilst their levels in both visceral fat tissues (Fig. 3a-d) remain relatively constant throughout our ageing cohorts of (lean) male chow-fed mice, they are progressively reduced by a HCD diet. ES-62 treatment provides significant protection against this decline, particularly in retroperitoneal fat where there is no significant difference in the levels of eosinophils between chow and ES-62-HCD-fed male mice at either d160 or d500. By contrast, the levels of visceral fat eosinophils were even higher in female HCD-PBS mice at d160 than those found in young lean female mice. These elevated levels were further enhanced in the female HCD-ES-62 mice at d160, although the levels of eosinophils in both female HCD cohorts declined to below those in chow mice between d340-500; nevertheless, even at these later time points, ES-62 still increased eosinophil levels relative to those seen in the gonadal fat of the female HFD-PBS group (Fig. 3a-d).

These gender- and tissue-specific effects presumably reflected ES-62 recruitment of differential homeostatic mechanisms capable of counteracting HCD-induced adipocyte dysfunction: in female mice, this is associated with a rise in IL-4 and IL-5 mRNA expression in the gonadal (Fig. 3e & f), but not retroperitoneal (results not shown) fat of such animals at d160. HCD-induced changes in adipose metabolic function have been associated with disruption of the phenotypic balance of M1/M2-like adipose tissue macrophages (ATM), typically resulting from an increase/recruitment in M1-like (CD11c+CD301b-/CD206-), which can be counteracted by the protective actions of eosinophils repolarising macrophages

towards an M2 (CD11c-CD301b+/CD206+)-like phenotype in an IL-4/5-dependent manner. Our analysis did not reveal a clear ES-62 repolarisation of these macrophage populations in either adipose tissue from male or female HCD mice during ageing. However, corresponding with the increased eosinophils and type-2 cytokines (IL-4 and IL-5) observed in gonadal tissue from female, but not male, HCD-fed mice at d160, there is a greater increase in M2 (CD11c-CD301b+)-like macrophages in both PBS- and ES-62-treated female HCD mice than in the male HCD cohorts, which instead displayed a strong rise in M1 (CD11c+CD301b-)-like macrophages (Fig. 3g & h). Nevertheless, it is increasingly evident that M1- and M2-like phenotypes are heterogeneous and that (pathological) hybrid M1-M2 phenotypes develop during obesity[30,31]. Thus, a CD11c+ subset has been identified in gonadal and subcutaneous fat that co-expresses the M2-like marker, CD301b and has been proposed to maintain blood glucose and body weight in lean and obese mice, as evidenced by depletion of these cells preventing weight gain (and even promoting weight loss under conditions of obesity) and insulin resistance[32]. Likewise, CD11c+CD206+ macrophages have been associated with progressing inflammation and insulin resistance during obesity[33,34]. Consistent with this, we found CD11c+CD301b+ macrophages to be increased in gonadal fat (Fig. 3i) and, albeit not significantly, in retroperitoneal fat from all male and female HCD-fed groups at d160. Intriguingly, therefore, whilst CD11c-CD301b+ cells are depleted in the retroperitoneal fat of male, but not female, HCD-fed mice relative to normal chow controls, exposure to ES-62 restores these M2-like cells back to the levels in the male chow mice (Fig. 3j). These distinct gender- and fat tissue-specific responses to HCD may potentially underlie the differential effects of ES-62 on male and female longevity under conditions of diet-induced obesity, especially when considered in the

context that increased intra-abdominal visceral fat appears to play an particularly important role in driving obesity-associated pathologies in men, relative to women[35].

Adipocyte Dysfunction and Insulin Resistance

Adipocyte hypertrophy and hyperplasia has been reported to lead to insulin resistance and liver fibrosis via dysregulation of adipokines like leptin and adiponectin[4,6]. Whilst leptin normally acts to suppress appetite and adiponectin promotes insulin sensitivity, elevated leptin levels in human obesity appear to reduce adiponectin sensitivity. Consistent with this, whilst serum levels of leptin remained constant in the ageing male and female lean cohorts, although variable amongst individuals, leptin levels rose progressively in ageing male HCD mice and, quite dramatically between d340 and 500 in female HCD-fed mice: these rises were blocked in ES-62-treated mice, where leptin levels were not significantly different from those observed in chow-fed animals (Fig. 4a & b). By contrast, the rise in serum adiponectin observed with age in lean mice (males and females) was abolished by intake of a HCD diet and even suppressed below basal levels in male HCD mice, with ES-62 exhibiting only marginal effects on adiponectin levels (Fig. 4c & d).

Consistent with these adipokine effects contributing to insulin resistance, and again as observed in human obesity, serum insulin levels were substantially elevated in female and particularly, male HCD mice: however, this dysregulation was not modulated by ES-62. Interestingly, aged (d500) female, but not male, chow-fed mice show elevated serum insulin levels that are not significantly different to those of their age-matched HCD-fed cohorts (Fig. 4e & f). Reflecting these changes, increased fasting glucose levels and impaired glucose clearance (as indicated by their glucose

tolerance test [GTT] responses) were evident in HCD- but not chow-fed mice from d160 onwards (Fig. 4g & h). Although ES-62 slightly attenuated the age-associated rise in fasting glucose levels observed in ageing female HCD-fed mice, it did not protect against the defective glucose clearance observed following administration of a bolus of glucose in these mice, relative to their chow-fed controls (Fig.4i & j). This defect in glucose clearance is slight when compared to that widely documented for female mice fed a HCD acutely (up to ~10 weeks), likely reflecting the remodeling of glucose handling reported to result from the increased adipose tissue providing novel glucose sinks in mice fed a chronic HCD[36]. What is striking here is the dramatic remodelling of this response in male relative to female HCD-fed mice indicating quite different gender-dependent metabolic responses to obesity and increased adipose tissue during normal ageing (chow d500): ES-62 did not modulate glucose tolerance in either male or female HCD-fed mice (Fig. 4i-l).

Homeostatic model assessment of insulin resistance (HOMA-IR), a test designed to assess IR and pancreatic β-cell function, confirmed that HCD-fed mice, particularly the male cohorts, progressively developed IR and this was not prevented by ES-62. Again, we found substantial differences between the male and female cohorts, with the female, but not male, d500 chow-fed group exhibiting analogous HOMA-IR responses to their age-matched HCD-fed counterparts (Fig. 5a & b). Analysis of pancreatic β-cell function revealed that male HCD-fed mice showed an increase in the size of the pancreatic islets and associated elevated β-cell insulin and α-cell glucagon expression followed by a sharp decline in each of these parameters between d340-500 (Fig. 5c-j). These data are consistent with the compensatory hyper-production of insulin and glucagon occurring in response to obesity-induced

IR, followed by the islet death and pancreatic failure of the pancreas associated with established T2D[4]. The male chow-fed group also showed increases in islet size and insulin and glucagon production at d500 suggestive of an emerging ageing-associated IR that is a common feature of ageing in mice and humans[3]. These IR effects were much less pronounced in female mice with the HCD cohort more mirroring the responses of the male chow group. ES-62 had only marginal effects on these pancreatic responses in either male or female HCD-fed mice.

ES-62 promotes liver health

HCD-mediated disruption of adipocyte health and induction of IR consequently impacts on liver function[37], causing mitochondrial dysfunction and REDOX imbalance, which coupled with inflammation and fat and collagen deposition, leads to liver steatosis and fibrosis associated with the high incidence of liver tumours observed in our HCD-fed cohorts (Supplementary Tables 2 & 3). Consistent with this, HCD and ageing impaired respiration rates within isolated liver mitochondria of both male and female mice. ES-62 partially rescued the HCD diet-induced impairment in mitochondrial function in male mice at d160 but the beneficial effect of ES-62 on mitochondrial function was not observed at older ages (Fig. 6a & b; Supplementary Figure 4). In female mice, the effect of ES-62 on mitochondrial respiration rates was much less pronounced, although ES-62 similarly increased ADP-driven respiration rates at 160d. Such beneficial effects were not reflected by protection against the HCD-accelerated decrease in cytochrome C expression (Fig. 6c & d) previously associated with age-dependent decreases in mitochondrial respiratory capacity[38]. Rather, HCD-exacerbation of mitochondrial dysfunction was accompanied, particularly in the livers from female mice, by a transient increase in

HMOX1 expression (d160) and superoxide dismutase (SOD) and protein carbonylation activities (both d340) in the HCD relative to the chow cohorts, which displayed low levels of these REDOX activities (particularly SOD) at all timepoints (Fig. 6e-j). The delay in ageing-associated mitochondrial dysfunction by ES-62 in male HCD-fed mice was not associated with any modulation of these factors: rather, ES-62 further increased HMOX1 expression and decreased the SOD and protein carbonylation activities in female HCD-fed mice, setting them at levels comparable to that seen in both PBS- and ES-62-treated male HCD-fed cohorts.

Whilst steatosis slowly occurred in ageing male chow-fed mice, there was a more substantial increase in the female cohort over the 500 days of the study (Fig. 7a-d). However, reflecting the impact of HCD on adipose tissue, there was a dramatic but transient increase in the levels of fatty liver observed by d160 in both male and female HCD-fed mice that then appeared to resolve/remodel, resulting in similar levels of fatty liver being exhibited by the chow and HCD-fed mice at d500. The transient nature of the liver steatosis might support the idea of an age window in which the liver may be sensitive to pathology[39]. Certainly, paralleling the dramatic increase in liver fat deposition at d160, transient spikes in inflammatory cytokine (IL-1β and IL-18) and associated NLRP3 expression generally occurred within livers from HCD-fed mice before returning towards, or below, the stable basal levels observed in their chow counterparts by d500 (Fig. 7e-j). Reflecting its marginal protective effects on liver steatosis at d500, ES-62 only slightly reduced some of these inflammasome responses at d340 and d500 (Fig. 7e-j). Consequent to the spikes in liver steatosis and inflammation, we observed substantial acceleration and enhancement of age-related liver fibrosis (as evidenced by collagen deposition) in

both male and female HCD-fed mice. Critically, exposure to ES-62 ameliorated HCD-induced liver fibrosis, maintaining the slow kinetics and low extent of age-related liver fibrosis seen in the chow-fed cohorts (Fig. 7k-n).

ES-62 acts to maintain gut integrity and prevent inflammation

ES-62 therefore appears to exert (differential) protective effects on metabolic tissues from both male and female HCD-fed mice that should contribute to improved healthspan in both genders, but do not at this stage fully explain its extension of lifespan in male HCD mice. To further investigate the potential reason for this sexual-dimorphic response we investigated the effect of ES-62 treatment on HCD-induced gut inflammation and loss of barrier integrity and associated dysbiosis of the microbiome that has not only been directly linked to the development of visceral fat inflammation, IR and obesity[40,41] but also to lifespan[42,43]. Emerging evidence from Drosophila suggests that lifespan is limited by gut pathology such that intestinal epithelial barrier integrity appears to be a more effective predictor of mortality than chronological age[44,45]. Indeed, it has been proposed that the extension of lifespan in response to dietary restriction (DR) in female flies may reflect DR's ability to reduce their profound gut pathology observed during ageing[46].

In our analysis, we focused on the ileum and colon not only because these are the sites of induction of effector and regulatory inflammatory cells, respectively but also because the colon contains the highest diversity of abundance of microbiota in the gut. HCD was found to accelerate and worsen the ileum pathology occurring during ageing seen in chow-fed mice in terms of an overall pathology score (scoring based on degree of cellular infiltration, epithelial erosion and villus atrophy[47]) as well as

quantitative analysis of villi length, basal lamina thickness and collagen deposition in both male and female mice (Fig. 8a-f; Supplementary Fig. 5a-d). ES-62 afforded some protection against these pathological changes, slowing the age-associated shortening in villi length in male and female mice as well as delaying the age-associated increase in pathology in female mice. By contrast, analysis of colon tissue showed ES-62 acted to slow the induction of pathology and prevent the changes in crypt morphology (ratio of crypt depth to intercrypt width[47,48]) in male but not female mice (Fig. 8g-l).

Furthermore, reflecting the cellular infiltration and inflammation identified in the pathology scoring, whilst the male mice in the HCD cohort exhibited increased levels of IL-17 expression in colon tissue relative to their chow-fed counterparts, this was abrogated by their exposure to ES-62. By contrast, colonic IL-17 expression similarly progressively increased with ageing in female mice, irrespective of diet or exposure to ES-62 (Fig. 9a-c). Age (autoimmunity) associated B cells (ABCs; CD19+CD21-CD23-CD11c+ B cells) have been proposed to promote TH1/TH17-mediated inflammation (and autoimmunity) during ageing, although they have also been reported to play roles in protective immunity particularly with respect to viral infection[49,50]. Levels of these circulating cells are increased in the spleens of d500 mice (Fig. 9d & e), particularly, and as reported previously in the female cohorts[49,50]. Their accumulation is accelerated by HCD and this is not prevented by ES-62: rather, perhaps reflecting their reported relatively high phosphorylcholine (PC)-reactivity, they are increased in both the male and female ES-62-treated HCD-treated cohorts. This may simply reflect the increased levels of anti-PC antibodies arising as a consequence of chronic exposure to the PC-containing ES-62 in these

cohorts (Fig. 9f-i) but which could possibly help to protect against bacterial infection in old age[51]. However, analysis of CD19+IL-10+Bregs, cells that can act to resolve pathogenic inflammation[52] including that associated with perturbation of the gut microbiota[53] and obesity[54], showed that exposure to ES-62 increased their levels in the spleens of male (d340) and female (d500) HCD-fed mice (Fig.9j & k). Interestingly, and presumably via a homeostatic mechanism to control the emerging gut pathology in d500 chow-fed mice and its acceleration by HCD, whilst we find increased levels of CD19+IL-10+Bregs in the MLN of female chow-fed mice by d340-500, these levels peak in their HCD-fed counterparts at 160-340 before declining sharply at d500 (Fig. 9l & m). Although exposure to ES-62 does not increase the levels of CD19+IL-10+ B cells in the MLNs of such female HCD mice, they do not undergo the decline observed in the PBS-treated cohort at d500. By contrast, whilst there is little change in the levels of CD19+IL-10+ B cells of MLNs of chow- or PBS-treated HCD-fed male mice, exposure to ES-62 substantially increases the levels of these cells at d340.

ES-62 maintains gut microbiota homeostasis during HCD-induced ageing

Changes in the microbiome contribute to the loss of intestinal barrier integrity[40,41,55] during ageing and impact directly on obesity and longevity[42,43]. We have recently shown that the protection afforded by ES-62 against inflammatory arthritis is associated with normalisation of the gut microbiome and stabilisation of gut barrier integrity that prevents generation of pathogenic TH17-mediated inflammation and allows homeostatic resolution of inflammation by IL-10+ regulatory B cells in the collagen-induced arthritis model of rheumatoid arthritis in male mice[16].Thus, we investigated whether ES-62 acted to normalise the ageing microbiota and prevent

the dysbiosis resulting in loss of barrier integrity by metagenomic analysis of ileum plus colon faecal material, with samples from individual mice pooled to generate a representative cohort phenotype. Whilst generally stable in healthy adults, the gut microbiome can undergo dynamic changes particularly in early and late life and during inflammatory and metabolic disorders[56]. Consistent with this, we found profound differences at the phylum level in the microbiota not only amongst young and ageing male and female chow-fed mice, but also to a lesser extent between aged-matched chow- and HCD-fed mice, with ES-62 acting to normalise the impact of HCD back to chow levels, particularly in male mice (Fig. 9n, upper panels; day 340 data shown). There was a striking loss of Verrucomicrobia, particularly in female mice (Fig. 9n, lower panels, which exhibited unexpectedly high levels of these bacteria in the young (d56) control cohort and even the d340 female chow-fed group. Verrucomicrobia (primarily of the genus Akkermansia) are mucus-degrading commensals that have been reported to be a marker of gut health due to their ability to promote gut barrier integrity, Treg generation and insulin sensitivity[57,58]: thus, these findings may suggest, as with flies[46], that female C57BL/6J may be particularly vulnerable to (HCD-induced) gut pathology during ageing. The failure of ES-62 to restore these commensals, and promote Treg responses in general[9], may go some way to explaining why the helminth product does not extend lifespan in female HCD-fed mice but only in the male cohorts, which given their lower levels of Verrucomicrobia may be innately less susceptible to the pathological consequences of gut pathology. Certainly, there is sexual dimorphism in (microbiota-driven) immune responses and consequently, disease susceptibility with notably the stronger immune responses to infection evident in females predisposing them to chronic inflammatory disorders[59,60].

Typically, whilst the ratio of Bacteriodetes: Firmicutes increases from birth through to adulthood, it subsequently remains relatively stable in healthy individuals before decreasing in old age[61]: however, obese adults show a decreased Bacteroidetes: Firmicutes ratio relative to aged-matched lean individuals[43]. Reflecting this, whilst the proportions of Bacteriodetes:Firmicutes in the gut ileum and colon faecal matter of young lean male and female mice (d56; 14-20 human years[62,63]) are low, mid-life adult (day 340) chow-fed male and female mice exhibit an (equivalent) much higher Bacteriodetes:Firmicutes ratio which is reduced by some 65% in both genders when the mice are HCD-fed (Fig. 9o & p). However, whilst the proportions of Bacteroidetes:Firmicutes in the chow-fed mice declined in both sexes of the ageing d500 mice to the level exhibited by their HCD-fed counterparts, this is more pronounced in the male (by ~65%) relative to the female (by ~35%) cohorts, with the female HCD-fed female group apparently slowly increasing its Bacteroidetes:Firmicutes ratio throughout its lifespan. Exposure to ES-62 protects against the HCD-induced decreases in the Bacteroidetes:Firmicutes ratio in both male and female mice and indeed, maintains, or even increases, their proportional abundance in the oldest HCD-fed cohorts (male, ~75%; female, ~130%, relative to the “adult” d340 chow-fed animals; Fig. 9o & p) Moreover, increases in the proportions of Proteobacteria relative to Firmicutes have been associated with loss of gut barrier integrity and proposed to provide signatures of gut inflammatory disorders (e.g. inflammatory bowel disease) and ageing[56]. Interestingly, the Desulfovibrionaceae family of δ-Proteobacteria negatively correlate with longevity and have been shown to be reduced following dietary restriction (DR) in male C57BL/6 mice[64] whilst the Enterobacteriaceae (γ-Proteobacteria) are positively correlated with ageing-induced frailty in flies[55]. Consistent with these findings, we

found that whilst HCD-feeding induced ageing-related increases in the Desulfovibrionaceae family of δ-Proteobacteria in male and particularly, female mice, these were inhibited by exposure to ES-62 although in the case of female HCD mice, this reduction was only generally to around the level found in male HCD-fed mice (Fig. 9q). This male gender protective bias was more strikingly reflected in the finding that HCD induces a strong enrichment of the Enterobacteriaceae in ageing male but not female mice (d500) and that this outgrowth is essentially abrogated by exposure to ES-62 (Fig. 9r). Collectively, these data suggest that ES-62 acts to broadly normalise gut microbiome changes associated with ageing and loss of intestinal barrier integrity preferentially in male HCD-fed mice and this may be a contributor to protection against the decrease in lifespan resulting from dysregulation of immunometabolic pathways in chronic obesity.

Mathematical modelling of ageing "signatures" in chow- and HCD-fed mice

Our survival and cross-sectional intervention studies have highlighted a number of differential age-, gender-, diet- and/or ES-62-treatment responses in ageing mice that underline the need for identification of precise and relevant biomarkers to identify sites of potential intervention and appropriate stratified cohorts. To begin to address this, we have subjected our multidimensional data sets (98 pathophysiological, immunological and metabolic variables assayed in this study) to unsupervised mathematical modelling and statistical analysis to identify the key (differential) signatures associated with ES-62-mediated promotion of healthspan in male and female HCD-fed mice. Firstly, we validated our data set analysis by identifying the features most predictive of HCD-fed mice (Fig. 10a) and as expected, this revealed (with >95 % accuracy) increases in adiposity and liver damage as well

as adipokine responses associated with IR. Moving on to an examination of the gender differences in response to the HCD, this highlighted the inflammatory bias of female mice demonstrated in the experimental studies above (Fig. 10b). Reflecting this bias, prediction of the healthspan features most robustly associated with ES-62-treatment of female HCD-fed mice (Fig. 10c) revealed modulation of a panel of almost exclusively inflammatory markers (visceral fat eosinophils and type-1 [IL-1β, IL-18] and type-2, [IL-4, IL-5 and IL-10] cytokines. By contrast, whilst ES-62 treatment of male HCD-fed mice (Fig. 10d) was also associated with modulation of visceral fat eosinophils and associated type 2 cytokines, it also targeted immunoregulatory elements (Bregs) and signatures associated with health of gut and metabolic tissues. In conjunction with typing individual microbiota status, such analysis now directs our future studies examining the roles of these targets in promoting the extension of lifespan associated with treatment of male HCD-fed mice with ES-62.

Methods

Mouse husbandry: longevity and cross-sectional healthspan studies

Male and female C57BL/6J mice (Envigo, UK) were housed in the Central Research Facility (University of Glasgow, Scotland) and maintained at 22°C under a 12-hr light/dark cycle. All procedures were undertaken under a UK Home Office Project Licence (60/4504), following the “principles of laboratory animal care” (NIH Publication No. 86-23, revised 1985) and in accordance with local ethical committee guidelines. Lifespan (survival study) cohort mice (all groups n=24) were housed in same sex groups of 2 to 4 under specific pathogen-free conditions within individually ventilated cages (Techniplast, UK). Mice had *ad libitum* access to water and normal

chow until 10 weeks of age when the diet was switched to Western diet RD + 150 ppm Fenbendazole (SDS, UK), denoted high calorie diet (HCD). Mice were administered PBS or purified ES-62 (1 μg) weekly via the subcutaneous route from 9 weeks old. Endotoxin-free ES-62 was purified from spent culture medium as described in detail previously[65]. Individuals were monitored daily and weighed weekly, but otherwise left undisturbed until they died. Survival was assessed from 48 female (HCD-PBS, n=24; HCD-ES-62, n=24) and 48 male (HCD-PBS, n=24; HCD-ES-62, n=24) mice, with all animals dead by the time of this report. Kaplan-Meier survival curves were constructed using known birth and death dates, with differences between groups evaluated using the log-rank test. If death appeared imminent (as assessed by our humane end-points) mice were weighed, euthanized and examined for macroscopic pathological changes using previously described protocols[66,67] with this date considered date of death.

Additional cross-sectional healthspan cohorts of mice were sacrificed at 56 (Chow, n=6), 160 (HCD, n=10/group; Chow, n=6), 340 (HCD, n=12/group; Chow, n=6) and 500 (HCD, n=6/group; Chow, n=5) days of age and tissues were harvested for processing. At sacrifice, blood was collected and the serum isolated and stored at -20°C in endotoxin-free Eppendorf tubes. Liver was immediately removed post-mortem and prepared for Seahorse analysis. Blood, spleen, mesenteric lymph nodes and visceral (gonadal: epididymal and parametrial fat pads, and retroperitoneal: dorsal fat pad directly behind the kidneys and attached to the peritoneum proposed as relevant models for human intra-abdominal adipose tissue[68,69]) adipose tissue were prepared for flow cytometry analysis. Ileum and colon faecal contents and liver and visceral adipose tissues were collected in sterile endotoxin-free Eppendorf

tubes, snap frozen and stored at -80°C. In addition, all tissue samples were fixed in 10% neutral buffered formalin, and embedded in either paraffin or flash frozen in OCT and stored at -80°C for histological analysis.

Food intake, grip strength and body mass monitoring

A pre-weighed amount of food was administered via wire bar lid food hopper. The average consumption/mouse/day was calculated at the end of a 72-hour monitoring period monthly. Grip strength monitoring was carried out as per manufacturer's guidelines (Ugo Basile®, Italy) using a Gripometer, measuring the peak grip force (gf) of the front limbs. The mouse was lowered towards a t-shaped grasp bar, once the animal gripped the bar it was gently pulled away and the peak amplifier recorded the amount of resistance. An average of three measurements was described as the mean gf. Body weight was monitored twice weekly for the duration of the experiment.

Tissue processing, histology, and immunofluorescence

Paraffin embedded tissues were sectioned at 5-6 μm and OCT tissues were cryosectioned (Thermoscientific, UK) at 8-10 μm thickness between -14 to -30°C. All tissues were haematoxylin and eosin (H&E) stained, gut and liver tissue sections were stained with Gömöri's Trichrome using previously described methods [16]. Prior to immunofluorescence (IF) staining, antigen retrieval (10 mM citrate buffer, pH 6) was performed and the sections were avidin/biotin blocked (Vectorlabs, UK). Briefly, pancreatic insulin and glucagon were stained with rabbit anti-insulin (1/200 dilution, Catalogue number Ab181547 Abcam, UK) and rabbit anti-glucagon antibodies (1/200 dilution; Catalogue number Ab10988 Abcam, UK) overnight, followed by rat anti-mouse IgG Alexafluor 647 (1/400 dilution, Catalogue A28181 Invitrogen, UK) and

goat anti-rabbit IgG Alexafluor 488 (1/400 dilution, Abcam, UK). IL-17 was detected using goat anti-mouse IL-17 (1/100 dilution; Catalogue number Af-421-na R&D Systems, UK) followed by biotinylated rabbit anti-goat IgG (1/200 dilution; Catalogue number 31732 Invitrogen, UK) with streptavidin Alexafluor 647 (1/200; dilution Catalogue number S21374 Invitrogen, UK). IF sections were mounted with Vectashield with DAPI (Vectorlabs, UK) and images were acquired with an EVOS FL Auto 2 system (Thermofisher, UK).

Image quantification and analysis

Images were quantified with Volocity (PerkinElmer, USA) or ImageJ Software. The total pancreatic islet number and area (pixels) were quantified and total IF-labelled glucagon and insulin fluorescence (pixels) identified and thresholded across the entire field of view (FOV) using set intensity parameters. Liver fat droplet deposition was calculated as a percentage of thresholded “white area” relative to the total area of liver tissue in FOV. Adipose cell nuclei were identified, thresholded and counted using set intensity parameters and the particle analyser plugin. Adipocount software (CSBIO) was used to quantify the number and area of individual adipocytes in the field of view (FOV). In ileum and colon tissue basal lamina width, villi length (from crypt to tip) or crypt depth was measured in three separate areas in the FOV and averaged. Collagen deposition was quantified by identifying percentage green/blue staining in FOV using the ColourDeconvolution plugin. A gut tissue pathology scoring protocol (Supplementary Figure x) was developed from the methods described by Erben *et al*. (2014)[47]. Images were given an unbiased score for each described parameter. The overall pathology score was calculated (average of cellular infiltration-spatial, epithelial erosion and villus/crypt atrophy).

Glucose tolerance testing and HOMA-IR

Mice were fasted overnight prior to testing. Throughout the procedure blood samples were obtained via caudal vein venesection and measured using an accu-chek performa (Roche, UK) or OneTouch Ultra (Lifescan, UK) glucometer. A fasting glucose (mmol/L) measurement was taken prior to the intraperitoneal administration of 20% glucose solution (dosage 2g glucose/kg body mass) and subsequent glucose tolerance measurements were recorded at 15, 30, 60 and 120 minutes post injection, with the glucose tolerance expressed as the area under the curve (AUC) over this 120 minute period.

Serum insulin, leptin and adiponectin were assessed using the mouse metabolic and Adiponectin MSD kits as per manufacturer's guidelines (Meso Scale Diagnostics, USA). Insulin resistance was estimated using the homeostasis model assessment for insulin resistance (HOMA-IR) index using the formula described previously[70], HOMA-IR index = [fasting glucose (mmol/L) x fasting insulin (mIU/L)]/22.5)

Flow cytometry

Spleen, mesenteric lymph node (mLN), whole blood, and stromal vascular fraction (SVF) of gonadal and retroperitoneal adipose tissues were suspended in FACS buffer (2.5% BSA; 0.5 mM EDTA, in PBS) following red blood cell-lysis (eBioscience, UK). Adipose tissue was digested with 1 mg/ml collagenase type II (Sigma, UK) and passed through 100 μM cell filters to generate a single cell suspension. Cells were washed in FACS buffer and incubated with Fc block (Biolegend, UK) before staining with the relevant antibodies. For eosinophils, cells were analysed for SiglecF (PE: Catalogue number 552126 BD Bioscience, UK) and for macrophage phenotypes,

cells were measured for F4/80 (Biotin: Catalogue number 123105 with SA-ef780), CD301b (APC: Catalogue number 146813) or CD206 (APC: Catalogue number 141707) and CD11c (PeCy7: Catalogue number 117318) expression. Whole blood was red-cell lysed, washed in FACS buffer before incubation with Fc block and the relevant antibodies. Lymphocytes were incubated with antibodies specific for mouse CD3 (FITC or PE : Catalogue number 100203 or 100205), CD4 (PE: Catalogue number 100407 or APC-ef780: Catalogue number 47-0042-82 eBioscence, UK), CD8 (PeCy7: Catalogue number 25-0081-82, eBioscence, UK), CD45RB (FITC: Catalogue number 103305 or APC-ef780: Catalogue number 47-0451-82, Invitrogen, UK) and CD44 (PerCP: Catalogue number 103036). Lymphocytes from the spleen and mesenteric lymph nodes were labelled with antibodies specific for mouse CD19 (AF700: Catalogue number 115527), CD23 (PeCy7 or AF488: Catalogue number 101613 or 101609), CD21 (PE: Catalogue number 123409), CD11c (FITC or PeCy7: Catalogue number 117305 or 117318), IgD (PerCP/Cy5.5: Catalogue number 405709), IgM (Biotin: Catalogue number 406503; Strepavidin Bv450), IL-10 (PE: Catalogue number 505007). All antibodies were purchased from BioLegend, UK. Fixable viability stain (APC-ef780 or and v450: Catalogue number 65-0865-14 or 65-0863-14; Invitrogen, UK) was used to select for live cells and, for analysis of IL-10^{+} regulatory B cells (Bregs), lymphocytes were stimulated with PMA, ionomycin, Brefeldin A and LPS (Sigma, UK) as described previously[16]. Data were acquired using a BD LSRII flow cytometer and populations were gated using isotype and fluorescence minus one (FMO) controls using FlowJo, LLC analysis software (Tree Star/ BD).

Serum and antibody ELISA

Interleukin-1β (IL-1β), IL-6 and TNF-α expression in serum was determined by ELISA in line with manufacturer's guidelines (BD Biosciences, UK). Anti-PC-BSA IgG and IgM antibodies in serum[65] were quantified using a reciprocal end point dilution method. Briefly, high-binding 96 well ELISA plates were coated with PC-BSA overnight at 4°C before washing and blocking with 1% BSA/PBS. Serum was initially diluted 1:100 and then serially diluted three-fold until 1:218700, incubated with HRP-conjugated goat anti-mouse IgG or IgM (1:10,000;1:6,000) in 10% FBS/PBS prior to developing with TMB, stopping with 2M sulphuric acid and read at an optical density of 450nm.

Seahorse XF assay

The XF Mitostress assay (Agilent Technologies, UK) was performed as previously described[71]. Briefly, hepatic mitochondria were isolated and added to an XF culture plate at a concentration of 10 μg per well. A pre-soaked eXF cartridge was prepared[72] and the culture plate loaded into an XF24 Analyser (Agilent Technologies, UK) and the assay initiated. Oxygen consumption rate (OCR) was measured in substrate alone (10 mM pyruvate, 2 mM malate), during state 3 (ADP [4 mM]), state 4 (oligomycin [2.5 mg/ml]), state 3u (FCCP (carbonyl cyanide 4-(trifluoromethoxy) phenylhydrazone) [4 mM]), and lastly antimycin A with rotenone [40 mM]. All reagents were sourced from Sigma, UK.

Superoxide dismutase (SOD) and protein carbonyl (PC) activities were quantified in liver tissue homogenates using a Total SOD activity assay kit and Carbonyl assay kit, respectively in line with manufacturer's guidelines (Cayman Chemical Company, Estonia).

qRT-PCR

mRNA was extracted from liver, gonadal and retroperitoneal adipose tissue using the RNeasy Lipid Tissue mini kit (Qiagen, Germany), or tissue was lysed in QIAzol prior to mRNA extraction using the DNA away RNA extraction kit (NBS Biologicals, UK). mRNA was transcribed into cDNA using the High Capacity cDNA Reverse Transcriptase kit (Applied Biosystems, Life Technology, UK) for use with Applied Biosystems Quant Studio 7 and KiCqStart® qPCR ready mix (Sigma-Aldrich) and KiCqStart™ Primers. Data were normalized to the housekeeping gene β-actin to obtain the ΔCT values that were used to calculate the 2^-ΔCT. Primer sequences were β-actin (forward - GATGTATGAAGGCTTTGGTC, reverse - TGTGCACTTTTAT TGGTCTC), IL-1β (forward - GTGATATTCTCCATGAGCTTTG, reverse - TCTTCTT TGGGTATTGCTTG), IL-4 (forward - CTGGATTCATCGATAAGCTG, reverse - TTTG CATGATGCTCTTTAGG), IL-5 (forward - CCCTACTCATAAAAATCACCAG, reverse - TTGGAATAGCATTTCCACAG), IL-18 (forward - AAATGGAGACC TGGAATCAG, reverse - CCTCTTACTTCACTGTCTTTG), cytochrome C (forward - CCGGAACGAA TTAAAAATGG, reverse - TCTGTGTAAGAGAATCCAGC), HMOX-1 (forward - CATGAAGAACTTTCAGAAGGG, reverse - TAGATATGGTACAAGGAAGCC), NLRP3 (forward - GATGCTGGAATTAGACAACTG, reverse - GTACATTTCACCCAA CTGTAG) and TripBr2 (forward - CCACTTGTAACACACTCTTC, reverse - TCAACA TTAGCAACACAGTC).

Metagenomics

Genomic DNA was extracted from the ileum and colon faecal matter using the QIAamp DNA Stool Mini Kit (Qiagen). Colon and ileum DNA were combined for each individual mouse, and samples were pooled on a group basis for shotgun

metagenomic analysis using the Ion Torrent PGM™ platform. 100 ng of pooled DNA was fragmented and barcoded using the NEBNext® Fast DNA Fragmentation and Library Prep Set for Ion Torrent™ (NEB Inc, UK) and IonXpress Barcode Adapters kit (ThermoFisher Scientific) respectively. The quality and quantity of all barcoded DNA libraries were analysed using the High Sensitivity DNA analysis kit (Agilent, UK) on the 2100 Bioanalyzer Instrument and Qubit Fluorometer (ThermoFisher Scientific). Samples were prepared using the Ion PGM™ Hi-Q™ View OT2 and Ion PGM™ Hi-Q™ View Sequencing kits (ThermoFisher Scientific) and 4 barcoded libraries were combined per Ion 316™ Chip kit (ThermoFisher Scientific). Data was analysed using MG-RAST and the number of reads per phylum, class, order, family or genera of species of interest were normalized against all bacteria present. Sequencing runs can be accessed using MG-RAST IDs mgl675297, mgl675300, mgl675312, mgl675291, mgl675309, mgl675318, mgl675306, mgl675294, mgl675321, mgl675315, mgl675285, mgl675288, mgl675324, mgl675303.

Machine Learning

To identify the metabolic and immune variables most robustly associated with ES-62 treatment, sex, and diet, each of those groups was treated as classes in supervised machine learning classification. Predictors, or input matrix, consisted of 98 pathophysiological, immunological, and metabolic features determined from our cross-sectional chow- and HCD-fed male and female cohorts (comprising 158 mice, 79 males and 79 females). To preserve sample sizes, missing values were imputed using the median of all the available values from other mice for that feature. Each feature was then standardised by centring it around the mean and scaling to unit variance. Models were trained using 5-fold cross-validation on a 75% split of the full

dataset, and tested on the remaining unseen 25%. The performance of seven common algorithms was compared (logistic regression, naive Bayes, support vector machines, k nearest neighbours, decision tree, random forests, and gradient boosted trees). We chose to further tune the gradient boosted trees models for inference. Tuning of the gradient boosted trees entailed five rounds of repeated stratified 5-fold splits of the training set in each of which there was a randomised search of parameter space for column sampling size, learning rate, minimum child weight, number of estimators, and maximum tree depth. This generated an ensemble of tuned models from which we selected the best 15 models based on their accuracy in correctly classifying mice from the test set. We then used the resulting distribution of model outputs for ranking the importance of features (Gini index) in correctly classifying the test set mice. Machine learning was performed in Scikit-Learn[73] and associated plots using Seaborn[74].

Statistical Analysis

All data were analysed using GraphPad Prism 6 or 8 software using unpaired student T-tests, one or two-way ANOVA with Fishers LSD post-test for parametric data or Kruskal-Wallis test and Dunn's post-test for non-parametric data. For clarity, only significant differences between the HCD-PBS and HCD-ES-62 cohorts are shown on the figures, where significance is denoted by * = $p < 0.05$, ** = $p < 0.01$ and *** = $p < 0.001$.

Acknowledgements

The work was funded by linked awards to MMH and CS (BB/M029727/1) and WH (BB/M029662/1) from the Biotechnology and Biological Sciences Research Council.

Author contributions

JC, FL, JD, MAP and AT performed the experiments for the study designed by MMH, WH, CS and PAH. JD and FL manufactured ES-62. SB performed the Machine Learning and associated statistical analysis. MMH, WH and CS wrote the paper and all authors were involved in reviewing and revising the manuscript.

Conflicts of Interest

The authors have no conflicts of interest.

Figure Legends

Figure 1: ES-62 extends lifespan in male HCD-fed C57BL/6J mice. Kaplan-Meier survival curves (a) for male and female HFD-fed mice treated either with PBS or ES-62 (all groups n=24) were analysed as (a) mixed gender cohorts (PBS, n=48; ES-62, n=48); (b) male mice (PBS, n=24; ES-62, n=24, *$p<0.05$) only and (c) female mice (PBS, n=24; ES-62, n=24) only. The data for the male and female cohorts are also presented as the frequency distribution of lifespan (d, e). Longitudinal analysis of the body mass (BM; f), food intake (g) and grip strength (h) measurements of the individual mice was undertaken where data are presented as mean values ± SEM of the mice surviving at the indicated timepoints. Analysis of BM (i, j), gonadal fat (%BM; k, l), retroperitoneal fat (%BM; m, n) and liver (%BM; o, p) in male (i, k, m, o) and female (j, l, n, p) cross-sectional cohorts of chow (d56, n=6; d160, n=6; d340, n=6 and d500, n=5) and PBS- or ES-62-treated HCD (d160, n=10; d340, n=12 and d500, n=6) at cull. Data are presented as mean values ± SEM.

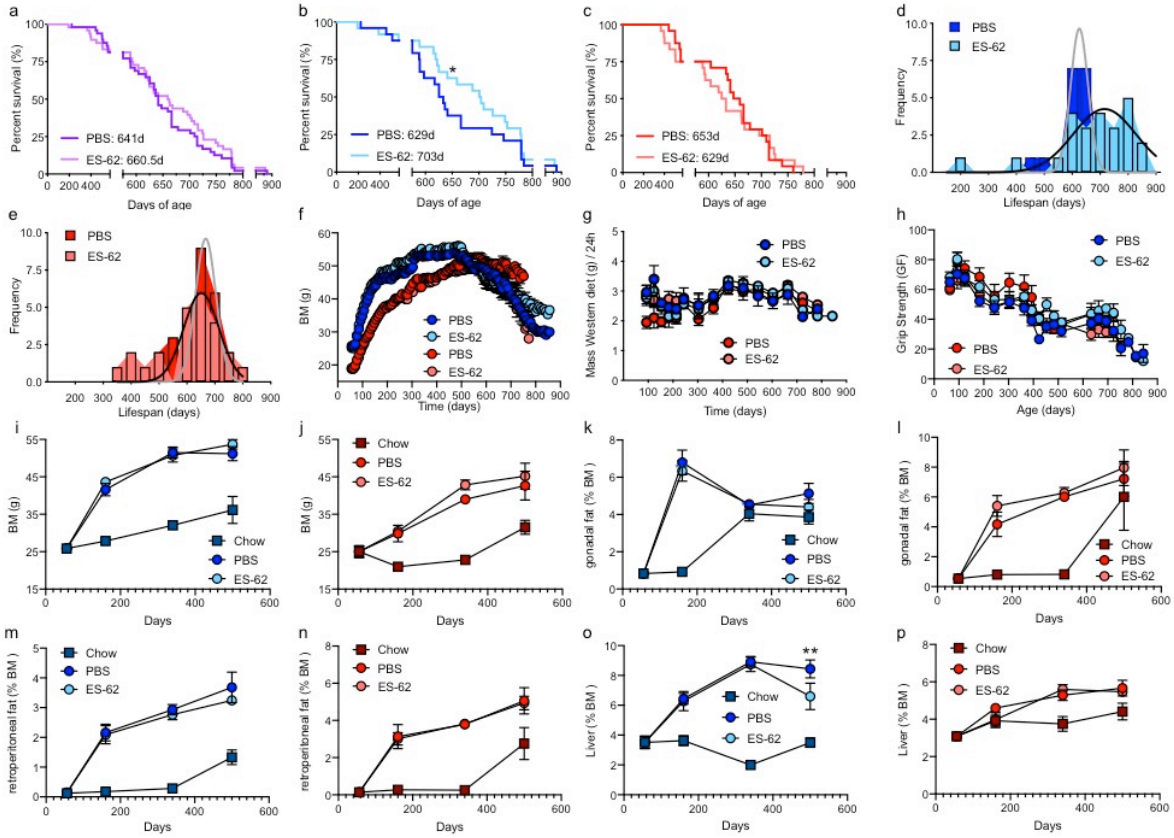
a
Percent survival (%)
PBS: 641d
ES-62: 660.5d
Days of age
b
Percent survival (%)
PBS: 629d
ES-62: 703d
*
Days of age
c
Percent survival (%)
PBS: 653d
ES-62: 629d
Days of age
d
PBS
ES-62
Frequency
Lifespan (days)
e
PBS
ES-62
Frequency
Lifespan (days)
f
BM (g)
PBS
ES-62
PBS
ES-62
Time (days)
g
Mass Western diet (g) / 24h
PBS
ES-62
PBS
ES-62
Time (days)
h
Grip Strength (GF)
PBS
ES-62
PBS
ES-62
Age (days)
i
BM (g)
Chow
PBS
ES-62
Days
j
BM (g)
Chow
PBS
ES-62
Days
k
gonadal fat (% BM)
Chow
PBS
ES-62
Days
l
gonadal fat (% BM)
Chow
PBS
ES-62
Days
m
retroperitoneal fat (% BM)
Chow
PBS
ES-62
Days
n
retroperitoneal fat (% BM)
Chow
PBS
ES-62
Days
o
Liver (% BM)
**
Chow
PBS
ES-62
Days
p
Liver (% BM)
Chow
PBS
ES-62
Days

Figure 2. ES-62 protects against visceral adipocyte hypertrophy in HCD-fed mice. Representative images (scale bar 100 μm) of gonadal fat from male (a) and female (b) chow- and HFD- (PBS or ES-62-treated) mice stained with H & E and resultant quantitative analysis of adipocyte size where data are presented as the mean values ± SEM, where n=4-5 individual male (c) and female (d) mice at each time point and the values for each mouse are means derived from n=3 replicate analyses. Representative images (scale bar 100 μm) of retroperitoneal fat from male (e) and female (f) chow- and HFD- (PBS- or ES-62-treated) mice stained with H & E and resultant quantitative analysis of adipocyte size where data are presented as the mean values ± SEM, where n ≥ 4 individual male (g) and female (h) mice and the values for each mouse are derived from n=3 replicate analyses. RT-qPCR analysis of TripBr2 expression in gonadal fat from male (i) and female (j) chow- and HFD- (PBS- or ES-62-treated) mice, where data are expressed as mean 2^ΔCT values ± SEM of individual mice and the values for each mouse are means of n=3 replicate analyses. Male cohort sizes: chow d56, n=6; d160, n=5; d340, n=6; d500, n=5; HFD-PBS d160, n=10; d340, n=11; d500, n=6; HFD-ES-62 d160, n=10; d340, n=12; d500, n=6 and female cohort sizes: chow d56, n=6; d160, n=5; d340, n=5; d500, n=5; HFD-PBS d160, n=8; d340, n=11; d500, n=6; HFD-ES-62 d160, n=10; d340, n=11; d500, n=6.

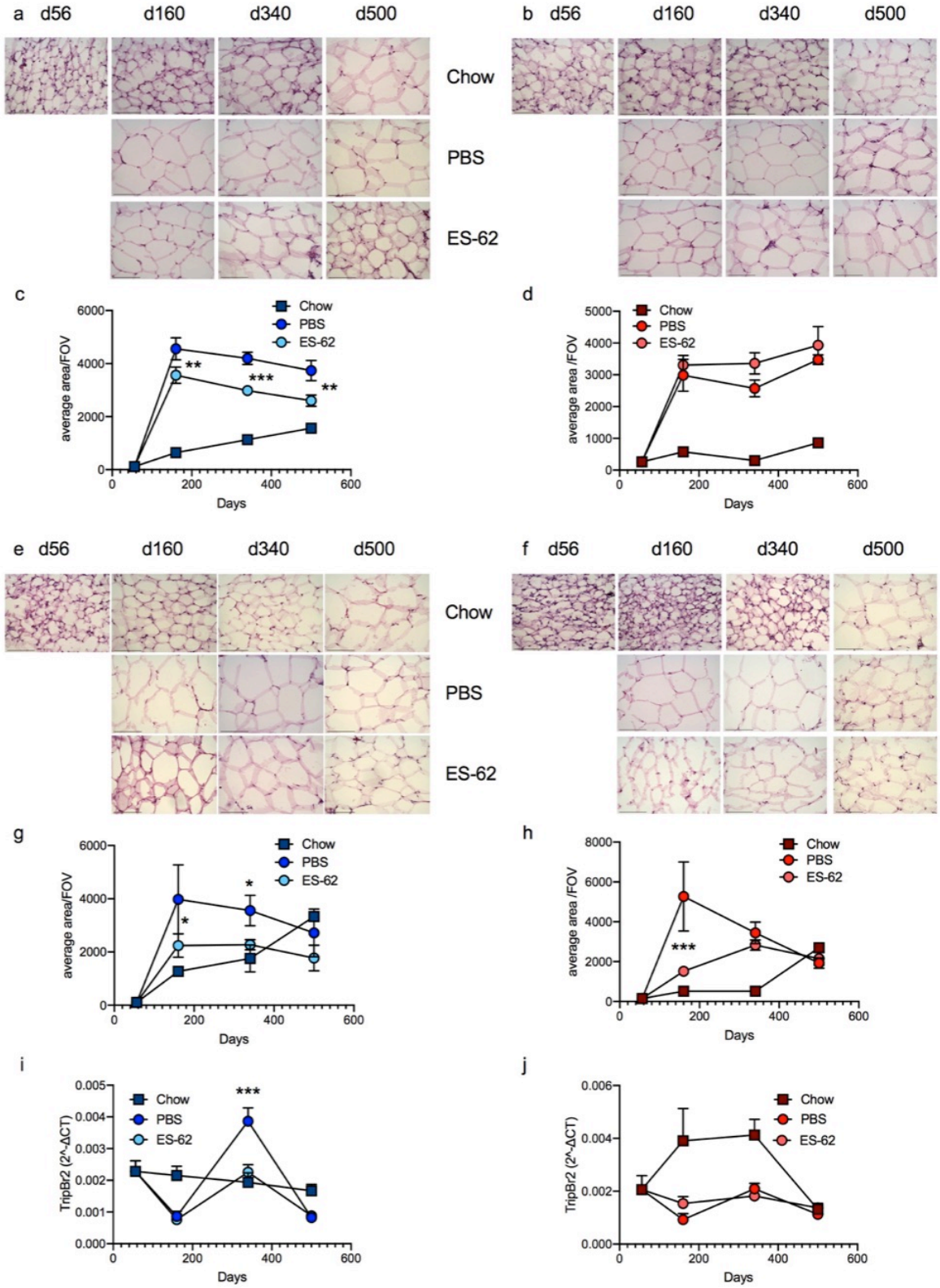
a d56 d160 d340 d500
Chow
PBS
ES-62
b d56 d160 d340 d500
c
average area/FOV
Days
Chow
PBS
ES-62
d
average area /FOV
Days
e d56 d160 d340 d500
f d56 d160 d340 d500
g
average area/FOV
Days
h
average area /FOV
Days
i
TripBr2 (2^-ΔCT)
Days
j
TripBr2 (2^-ΔCT)
Days

Figure 3. ES-62 promotes eosinophils and type-2 inflammatory responses in visceral adipose tissue in HCD-fed mice. The levels of SiglecF+ eosinophils (% SVF cells) from gonadal fat of male (a) and female (b) chow- and HFD- (PBS- or ES-62-treated) mice are presented as the mean values ± SEM at each time point where male cohort sizes: chow - d56, n=5; d160, n=3; d340, n=6; d500, n=5; HFD-PBS - d160, n=10; d340, n=11; d500, n=6; HFD-ES-62 - d160, n=9; d340, n=12; d500, n=6 and female cohort sizes: chow d56 - n=6; d160, n=6; d340, n=6; d500, n=5; HFD-PBS - d160, n=4; d340, n=11; d500, n=6; HFD-ES-62 - d160, n=6; d340, n=12; d500, n=6 and retroperitoneal fat of male (c) and female (d) chow- and HFD- (PBS- or ES-62-treated) mice are presented as the mean values ± SEM at each time point where male cohort sizes: chow - d56, n=5; d160, n=3; d340, n=5; d500, n=5; HFD-PBS - d160, n=9; d340, n=10; d500, n=6; HFD-ES-62 - d160, n=9; d340, n=12; d500, n=6 and female cohort sizes: chow - d56, n=6; d160, n=6; d340, n=6; d500, n=5; HFD-PBS - d160, n=4; d340, n=11; d500, n=6; HFD-ES-62 - d160, n=6; d340, n=12; d500, n=6. RT-qPCR analysis of IL-4 (e) and IL-5 (f) expression in gonadal fat from female chow- and HFD- (PBS- or ES-62-treated) mice where data are expressed as mean 2^ΔCT values ± SEM of individual mice and the values for each mouse are means of n=3 replicate analyses is presented. Cohort sizes: chow - d56, n=6; d160, n=5; d340, n=5; d500, n=5; HFD-PBS - d160, n=8 (IL-4), n=9 (IL-5) d340, n=11; d500, n=6; HFD-ES-62 - d160, n=9 (IL-4), n=10 (IL-5); d340, n=11; d500, n=6. The levels of F4/80+CD11c-Cd301+ (g, i) and F4/80+CD11c-Cd301+ (h, j) macrophages (% live SVF cells) in gonadal (g, h) and retroperitoneal (i, j) fat in male and female chow- and HFD- (PBS- or ES-62-treated) mice in the d160 cohorts are shown.

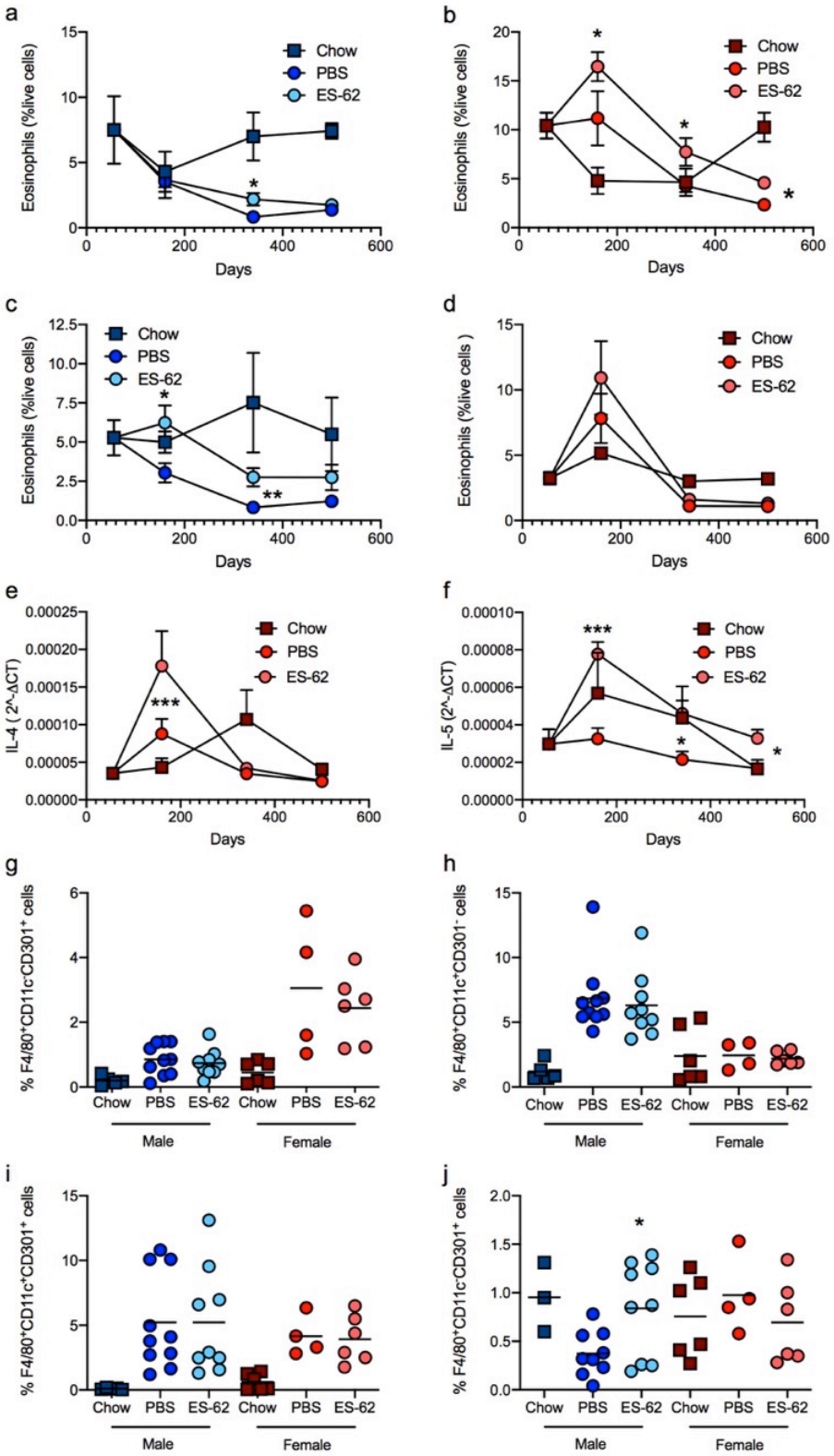
a
Eosinophils (%live cells)
Days
Chow
PBS
ES-62
b
Eosinophils (%live cells)
Days
Chow
PBS
ES-62
c
Eosinophils (%live cells)
Days
Chow
PBS
ES-62
d
Eosinophils (%live cells)
Days
Chow
PBS
ES-62
e
IL-4 (2^-ΔCT)
Days
Chow
PBS
ES-62
f
IL-5 (2^-ΔCT)
Days
Chow
PBS
ES-62
g
% F4/80+CD11c-CD301+ cells
Chow PBS ES-62 Chow PBS ES-62
Male
Female
h
% F4/80+CD11c+CD301- cells
Chow PBS ES-62 Chow PBS ES-62
Male
Female
i
% F4/80+CD11c+CD301+ cells
Chow PBS ES-62 Chow PBS ES-62
Male
Female
j
% F4/80+CD11c-CD301+ cells
Chow PBS ES-62 Chow PBS ES-62
Male
Female

F**igure 4. Effect of ES-62 on markers of Insulin Resistance (IR) in HCD-fed mice.** Serum levels of leptin (a, b), adiponectin (c, d) and insulin (e, f) from male (a, c, e) and female (b, d, f) chow- or HFD- (PBS- or ES-62-treated) mice at cull at the indicated time-points. Data are expressed as mean values ± SEM of individual mice. Male cohort sizes: chow - d56, n=5 (leptin), 6 (adiponectin, insulin); d160, n=6; d340, n=6; d500, n=5 (leptin, adiponectin), 4 (insulin); HFD-PBS - d160, n=9; d340, n=8 (leptin), 9 (adiponectin, insulin); d500, n=3 (leptin), 6 (adiponectin, insulin); HFD-ES-62 - d160, n=9; d340, n=7 (leptin), 9 (adiponectin, insulin); d500, n=3 (leptin), 6 (adiponectin, insulin) and female cohort sizes: chow - d56, n=6; d160, n=6; d340, n=5 (leptin), 6 (adiponectin); d500, n=3 (leptin), 5 (adiponectin, insulin); HFD-PBS - d160, n=9; d340, n=9; d500, n=4 (leptin), 6 (adiponectin, insulin); HFD-ES-62 - d160, n=9; d340, n=9; d500, n=4 (leptin), 6 (adiponectin, insulin). Measurement of fasting glucose (g, h) and glucose tolerance tests (GTT, i-l) were undertaken on male (g, i, k) and female (h, j, l) chow- and HFD- (PBS- or ES-62-treated) mice one week prior to cull at the indicated time-points and presented as AUC (i, j) for all timepoints and blood glucose levels (k, l) for the d500 cohorts. Data are presented as the mean values ± SEM of individual mice where male cohort sizes: chow - d56, n=6; d160, n=6; d340, n=6; d500, n=5; HFD-PBS - d160, n=10; d340, n=11; d500, n=6; HFD-ES-62 - d160, n=10; d340, n=12; d500, n=6 and female cohort sizes: chow - d56, n=6; d160, n=6; d340, n=5, d500, n=3; HFD-PBS - d160, n=9; d340, n=11; d500, n=6; HFD-ES-62 -d160, n=10; d340, n=12; d500, n=6.

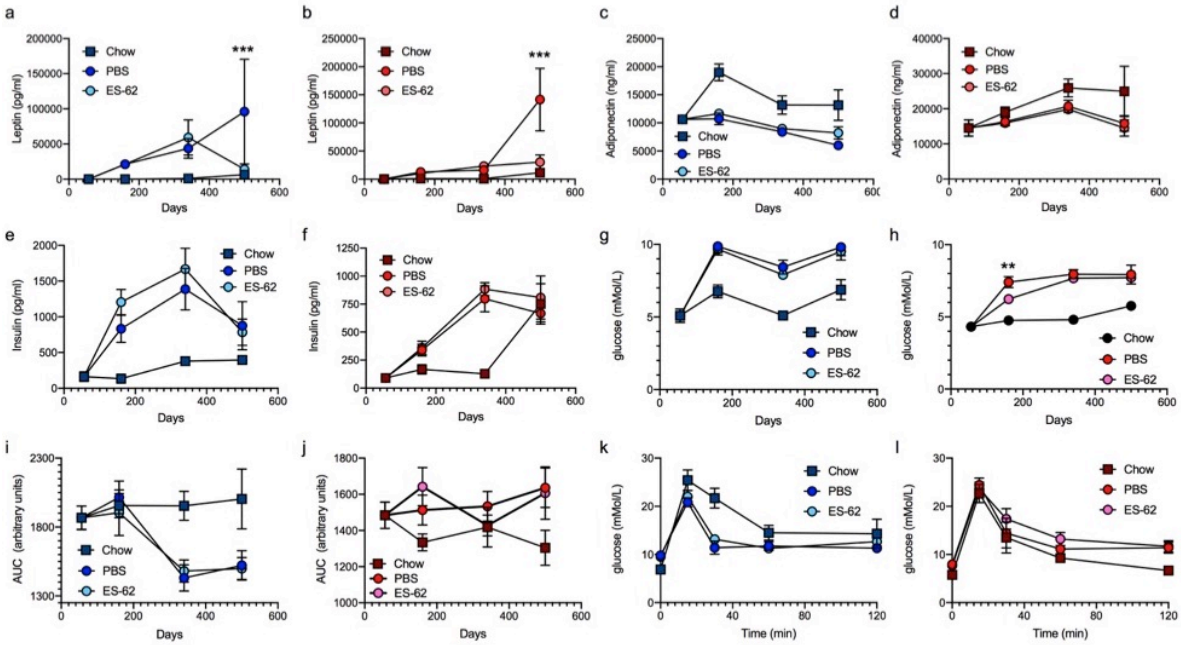
a
Leptin (pg/ml)
Days
Chow
PBS
ES-62
***
b
Leptin (pg/ml)
Days
Chow
PBS
ES-62
***
c
Adiponectin (ng/ml)
Days
Chow
PBS
ES-62
d
Adiponectin (ng/ml)
Days
Chow
PBS
ES-62
e
Insulin (pg/ml)
Days
Chow
PBS
ES-62
f
Insulin (pg/ml)
Days
Chow
PBS
ES-62
g
glucose (mMol/L)
Days
Chow
PBS
ES-62
h
glucose (mMol/L)
Days
**
Chow
PBS
ES-62
i
AUC (arbitrary units)
Days
Chow
PBS
ES-62
j
AUC (arbitrary units)
Days
Chow
PBS
ES-62
k
glucose (mMol/L)
Time (min)
Chow
PBS
ES-62
l
glucose (mMol/L)
Time (min)
Chow
PBS
ES-62

Figure 5: Effect of ES-62 on pancreatic function in HCD-fed mice. HOMA-IR determinations were made from fasting glucose and insulin levels in serum from male (a) and female (b) chow- or HFD- (PBS- or ES-62-treated) mice at cull at the indicated time-points. Data are presented as the values ± SEM of individual mice where male cohort sizes: chow - d56, n=6; d160, n=6; d340, n=6; d500, n=4; HFD-PBS - d160, n=9; d340, n=9; d500, n=6; HFD-ES-62 - d160, n=9; d340, n=9; d500, n=6 and female cohort sizes: chow - d56, n=6; d160, n=6; d340, n=5, d500, n=3; HFD-PBS - d160, n=9; d340, n=9; d500, n=6; HFD-ES-62 - d160, n=9; d340, n=9; d500, n=6. Representative images (scale bar 500 μm) of pancreas from male (c) and female (d) chow- and HFD- (PBS- or ES-62-treated) mice stained for insulin (green), glucagon (red) and counterstained with DAPI (blue). Quantitative analysis of islet size (e, f) and production of insulin (g, h) and glucagon (i, j) where data are presented as the mean values ± SEM are shown, where n=4-6 individual male (e, g, i) and female (f, h, j) mice at each time point and the values for each mouse are means derived from n=3 replicate analyses.

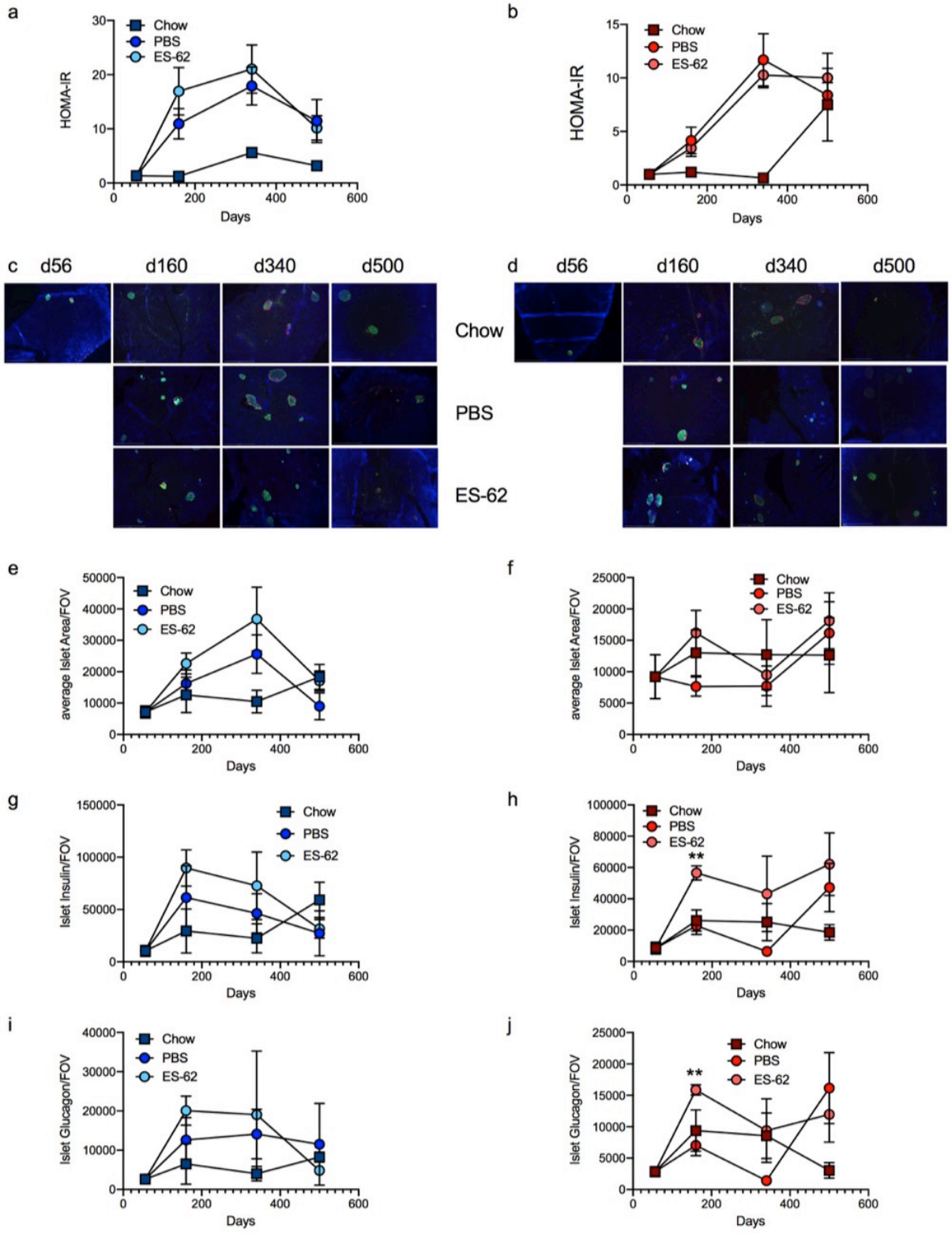
a
HOMA-IR
Days
Chow
PBS
ES-62
b
HOMA-IR
Days
Chow
PBS
ES-62
c
d56
d160
d340
d500
Chow
PBS
ES-62
d
d56
d160
d340
d500
e
average Islet Area/FOV
Days
Chow
PBS
ES-62
f
average Islet Area/FOV
Days
Chow
PBS
ES-62
g
Islet Insulin/FOV
Days
Chow
PBS
ES-62
h
Islet Insulin/FOV
Days
Chow
PBS
ES-62
**
i
Islet Glucagon/FOV
Days
Chow
PBS
ES-62
j
Islet Glucagon/FOV
Days
Chow
PBS
ES-62
**

Figure 6. ES-62 modulates liver function in HCD-fed mice. Mitochondrial respiration (oxygen consumption rate, OCR) was measured in livers from male (a) and female (b) chow- or HFD- (PBS- or ES-62-treated) mice at cull at d160. Data are presented as the values ± SEM of individual mice where cohort sizes were: male, chow n=6, HFD-PBS n=10 HFD-ES-62 n=9; female, chow n=5; HFD-PBS n=9; HFD-ES-62 n=10. RT-qPCR analysis of cytochrome C (c, d) and HMOX-1 (e, f) expression in liver from male (c, e) and female (d, f) chow- and HFD- (PBS- or ES-62-treated) mice are shown where data are expressed as mean 2^ΔCT values ± SEM of individual mice and the values for each mouse are means of n=3 replicate analyses. Male cohort sizes: chow - d56, n=6; d160, n=6; d340, n=6; d500, n=5; HFD-PBS - d160, n=10; d340, n=11; d500, n=6; HFD-ES-62 - d160, n=10; d340, n=12; d500, n=6 and female cohort sizes: chow - d56, n=6; d160, n=6; d340, n=6; d500, n=5; HFD-PBS - d160, n=5; d340, n=11; d500, n=6; HFD-ES-62 - d160, n=5; d340, n=12; d500, n=6. Determination of superoxide dismutase (SOD; g, h) and protein carbonylation (i, j) activities in liver from male (g, i) and female (h, j) chow- and HFD- (PBS- or ES-62-treated) mice where data are expressed as mean activity values ± SEM of individual mice. Male cohort sizes: chow - d56, n=6 (SOD), 3 (protein carbonylation); d160, n=6 (SOD), 3 (protein carbonylation); d340, n=6 (SOD), 3 (protein carbonylation); d500, n=5; HFD-PBS - d160, n=10 (SOD), 6 (protein carbonylation); d340, n=10 (SOD), 11 (protein carbonylation); d500, n=6; HFD-ES-62 - d160, n=8 (SOD), 6 (protein carbonylation); d340, n=10 (SOD), 12 (protein carbonylation); d500, n=6 and female cohort sizes: chow - d56, n=5 (SOD), 3 (protein carbonylation); d160, n=6 (SOD), 3 (protein carbonylation); d340, n=6 (SOD), 3 (protein carbonylation); d500, n=4; HFD-PBS - d160, n=9 (SOD), 6 (protein carbonylation); d340, n=10 (SOD), 9 (protein carbonylation); d500, n=6;

HFD-ES-62 - d160, n=10 (SOD), 6 (protein carbonylation); d340, n=10 (SOD), 11 (protein carbonylation); d500, n=6.

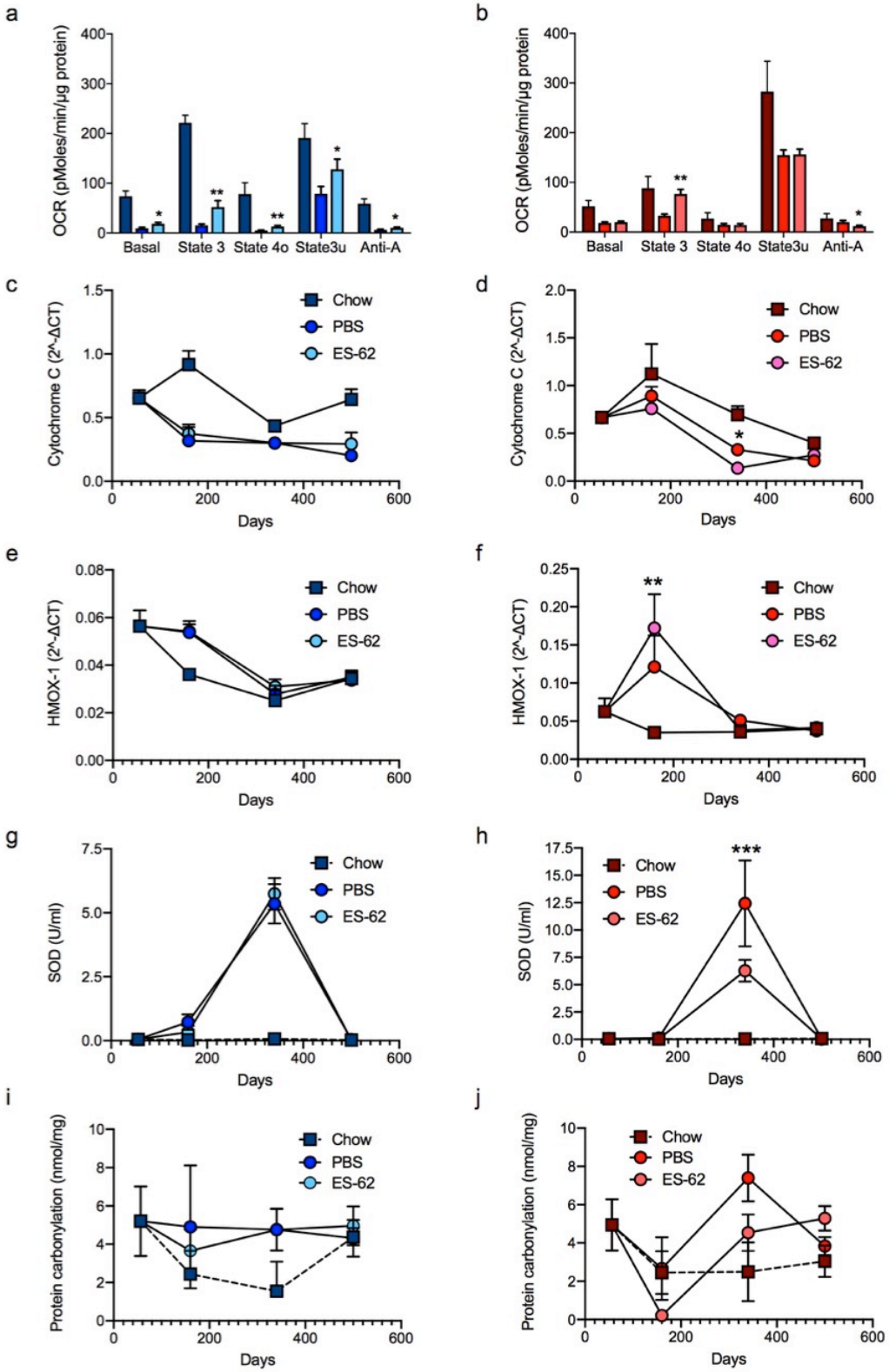
a
OCR (pMoles/min/µg protein)
Basal
State 3
State 4o
State3u
Anti-A
b
OCR (pMoles/min/µg protein)
c
Cytochrome C (2^-ΔCT)
Days
Chow
PBS
ES-62
d
Cytochrome C (2^-ΔCT)
e
HMOX-1 (2^-ΔCT)
f
HMOX-1 (2^-ΔCT)
g
SOD (U/ml)
h
SOD (U/ml)
i
Protein carbonylation (nmol/mg)
j
Protein carbonylation (nmol/mg)

Figure 7. ES-62 protects against liver fibrosis in HCD-fed mice. Representative images (scale bar 100 μm) of liver from male (a) and female (b) chow- and HFD- (PBS- or ES-62-treated) mice stained with H & E and resultant quantitative analysis of fat deposition where data are presented as the mean values ± SEM where n=5-6 individual male (c) and female (d) mice at each time point and the values for each mouse are means derived from n=3 replicate analyses. RT-qPCR analysis of IL-1β, IL-18 and NLRP3 expression in liver from female (e, f, g) and male (h, i, j) chow- and HFD- (PBS- or ES-62-treated) mice where data are expressed as mean 2^ΔCT values ± SEM of individual mice and the values for each mouse are means of n=3 replicate analyses. Male cohort sizes: chow - d56, n=6; d160, n=6; d340, n=6; d500, n=5; HFD-PBS - d160, n=10; d340, n=11; d500, n=6; HFD-ES-62 - d160, n=10; d340, n=12; d500, n=6 and female cohort sizes: chow - d56, n=6; d160, n=6; d340, n=6; d500, n=5; HFD-PBS - d160, n=5; d340, n=11; d500, n=6; HFD-ES-62 - d160, n=5; d340, n=12; d500, n=6. Representative images (scale bar 100 μm) of liver from male (k) and female (l) chow- and HFD- (PBS- or ES-62-treated) mice stained with Gömöri's Trichrome and resultant quantitative analysis of collagen deposition where data are presented as the mean values ± SEM, where n=5-6 individual male (g) and female (h) mice and the values for each mouse are derived from n=3 replicate analyses are presented.

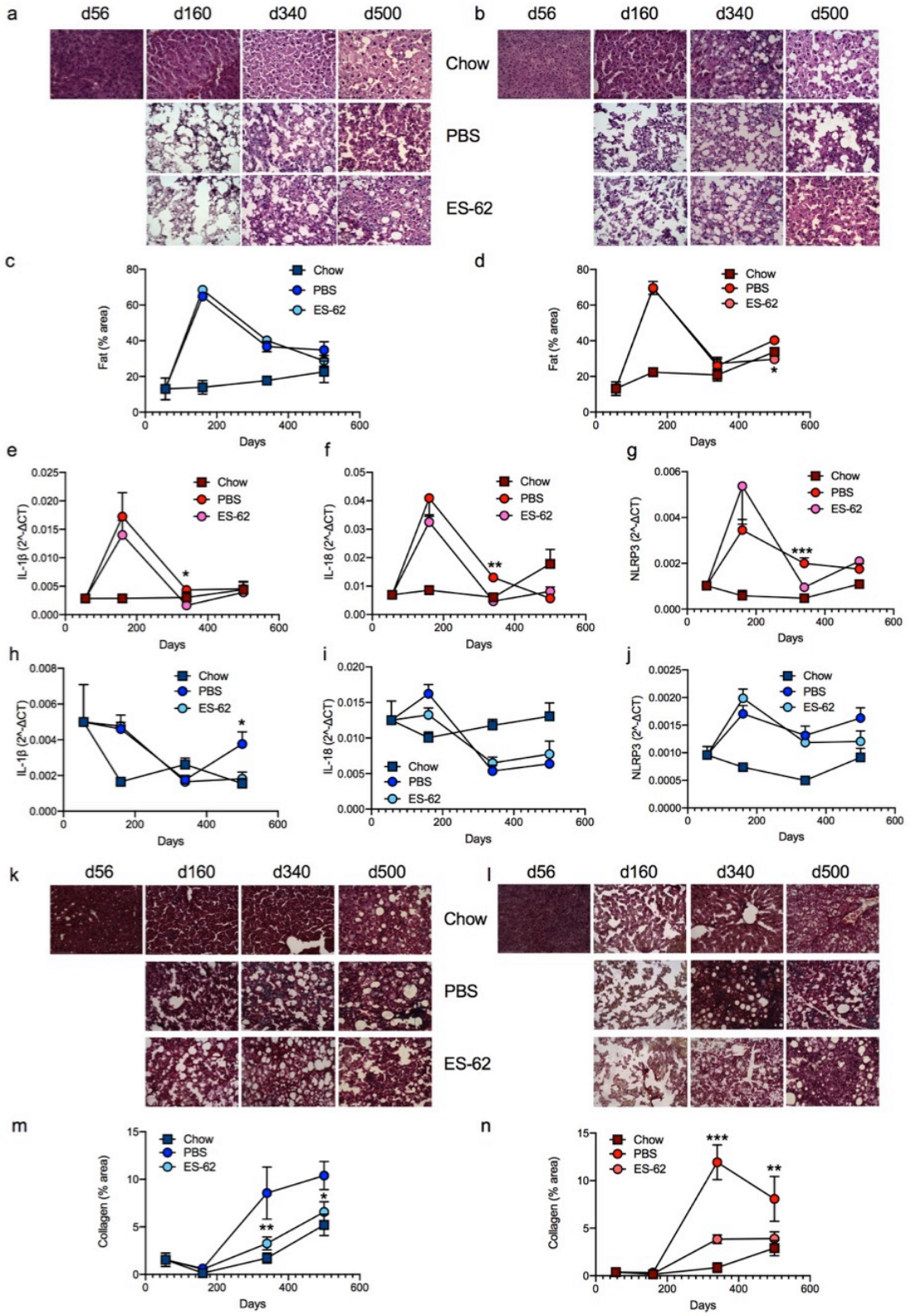
a
d56
d160
d340
d500
Chow
PBS
ES-62
b
c
Fat (% area)
Days
d
e
IL-1β (2^-ΔCT)
f
IL-18 (2^-ΔCT)
g
NLRP3 (2^-ΔCT)
h
i
j
k
l
m
Collagen (% area)
n

Figure 8. ES-62 protects against gut pathology in HCD-fed mice. Representative images (scale bar 500 μm) of ileum tissue from male (a) and female (b) chow- and HFD- (PBS- or ES-62-treated) d340 mice stained with H & E (upper panels) and Gömöri's Trichrome and resultant pathology scoring (c, d) and quantitative analysis of ileum length (e, f) are shown. Data are presented as the mean values ± SEM where n=4-6 individual male (a, c, e) and female (b, d, f) mice at each time point and the values for each mouse are means derived from n=3 replicate analyses. Representative images (scale bar 500 μm) of colon tissue from male (g) and female (h) chow- and HFD- (PBS- or ES-62-treated) d340 mice stained with H & E (upper panels) and Gömöri's Trichrome and resultant pathology scoring (i, j) and quantitative analysis of the ratio of crypt depth:intercrypt width (k, l) are shown. Data are presented as the mean values ± SEM where n=4-6 individual male (g, i, k) and female (h, j, l) mice at each time point and the values for each mouse are means derived from n=3 replicate analyses.

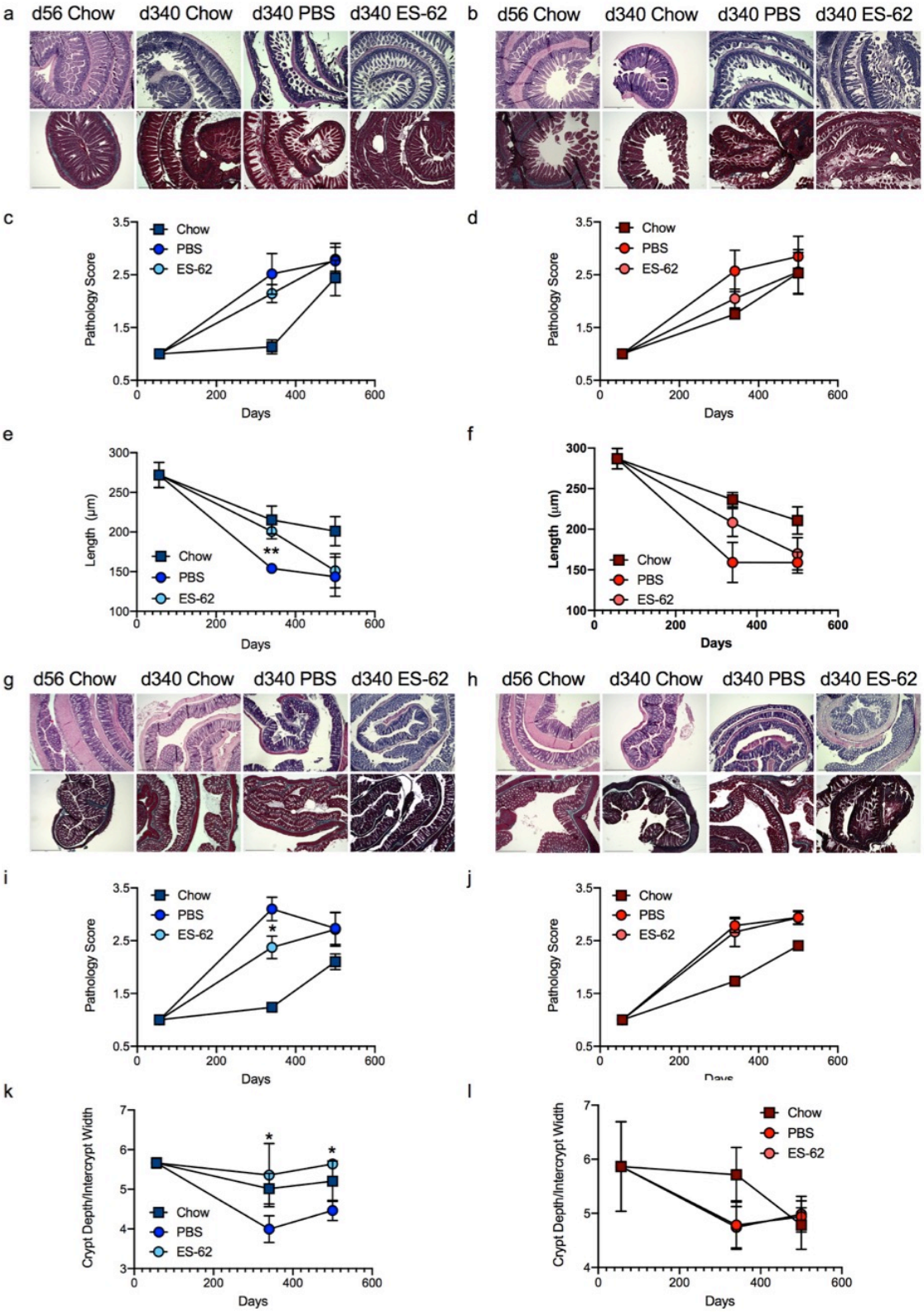
a
d56 Chow
d340 Chow
d340 PBS
d340 ES-62
b
c
Pathology Score
Days
Chow
PBS
ES-62
d
e
Length (µm)
**
f
g
h
i
*
j
k
Crypt Depth/Intercrypt Width
l

Figure 9. ES-62 acts to normalise the gut microbiome in HCD-fed mice. Representative images (scale bar 200 μm) of colon tissue (a) from male chow- and HFD- (PBS- or ES-62-treated) d500 mice stained for IL-17 (red) and counterstained with DAPI (blue) are presented. Quantitative analysis of colon IL-17 expression from male (b) and female (c) chow- and HFD (PBS or ES-62-treated) mice where data are presented as the mean values ± SEM, where n=4-6 individual mice at each time point and the values for each mouse are means derived from n=3 replicate analyses. Proportions of ABC (CD19+CD21-CD23-CD11c+) B cells (% live cells) in spleens of male (d) and female (e) chow- and HFD- (PBS- or ES-62-treated) mice are presented as the mean values ± SEM at each time point where male cohort sizes: chow - d56, n=6; d160, n=6; d340, n=6; d500, n=5; HFD-PBS - d160, n=6; d340, n=7; d500, n=6; HFD-ES-62 - d160, n=6; d340, n=8; d500, n=6 and female cohort sizes: chow - d56, n=5; d160, n=6; d340, n=6; d500, n=3; HFD-PBS - d160, n=9; d340, n=11; d500, n=6; HFD-ES-62 - d160, n=10; d340, n=12; d500, n=6. Serum titres (reciprocal end-point dilutions) of anti-PC IgM (f, h) and IgG (g, i) antibodies from male (f, g) and female (h, i) chow- and HFD- (PBS- or ES-62-treated) mice are presented as the mean values ± SEM at each time point where male cohort sizes: chow - d56, n=6; d160, n=6; d340, n=6; d500, n=5; HFD-PBS - d160, n=6; d340, n=10 (IgM), 11(IgG); d500, n=6; HFD-ES-62 - d160, n=9; d340, n=11; d500, n=6 and female cohort sizes: chow - d56, n=5; d160, n=5 (IgM), 6 (IgG); d340, n=5 (IgM), 6 (IgG); d500, n=5 (IgM), 3 (IgG); HFD-PBS - d160, n=7(IgM), 8 (IgG); d340, n=8 (IgM), 7 (IgG); d500, n=6; HFD-ES-62 - d160, n=8; d340, n=10 (IgM), 11 (IgG); d500, n=6. Proportions of Breg (CD19+IL-10+) B cells (% live cells) in spleens (j, k) and MLNs (l, m) of male (j, l) and female (k, m) chow- and HFD- (PBS- or ES-62-treated) mice are presented as the mean values ± SEM at each time point where

male cohort sizes: chow - d56, n=6; d160, n=6; d340, n=6; d500, n=5; HFD-PBS - d160, n=10; d340, n=11 (splenic), 7 (MLN); d500, n=6; HFD-ES-62 - d160, n=10; d340, n=12 (splenic), 8 (MLN); d500, n=6 and female cohort sizes: chow - d56, n=5 (splenic) 6 (MLN); d160, n=6; d340, n=5 (splenic), (6 (MLN); d500, n=5 (splenic), 4 (MLN); HFD-PBS - d160, n=9; d340, n=10; d500, n=6 (splenic), 5 (MLN); HFD-ES-62 - d160, n=10 (splenic), 9 (MLN); d340, n=12 (splenic), 10 (MLN); d500, n=6. The composition of bacterial phyla present in gut (ileum plus colon) faecal matter (n) of male and female chow- (d56 and d340) and HFD- (PBS- or ES-62-treated; d340) mice presenting proportion values as pie charts using pooled samples to represent each cohort. The Bacteroidetes:Firmicutes ratio (o, p) and levels of Desulfovibrionaceae (q) and Enterobacteriaceae (r) present in gut (ileum plus colon) faecal matter of male (o, q, r) and female (p, q, r) chow- (d56 and d340) and HFD (PBS or ES-62-treated) mice (each determined as proportion values) using pooled samples to represent each cohort are shown.

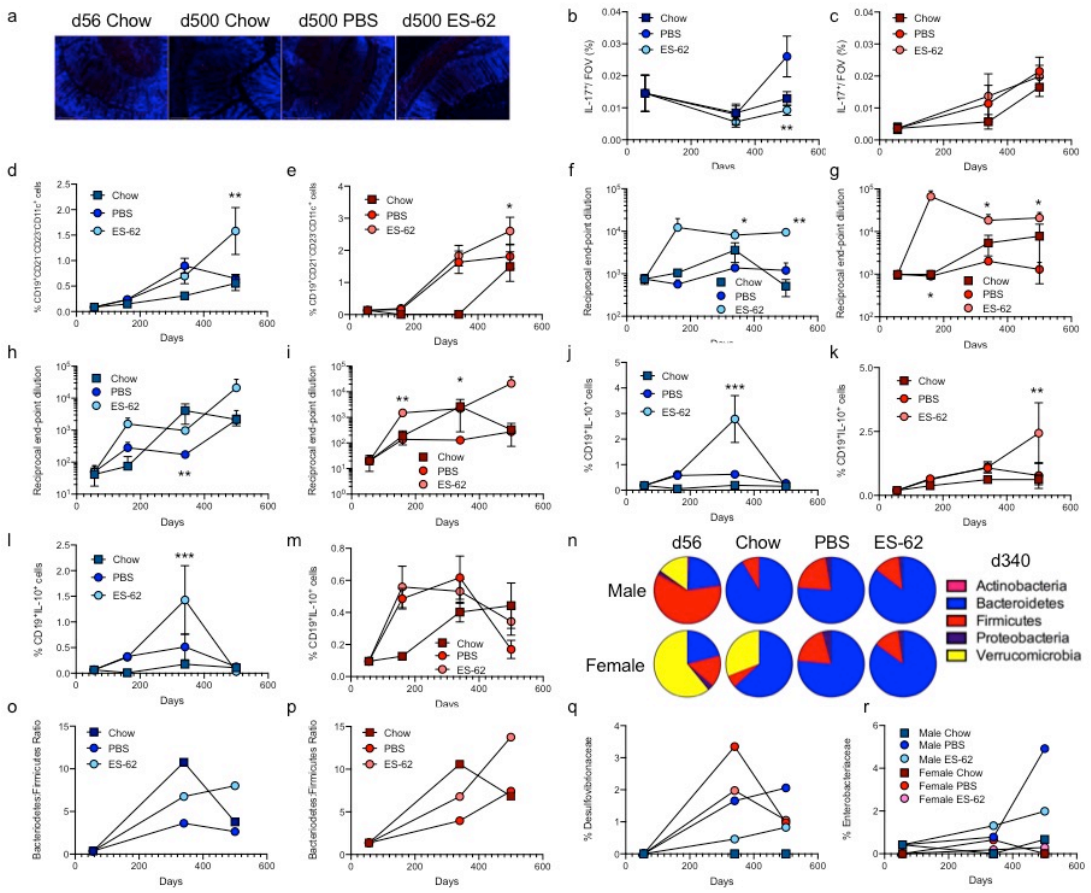
a
d56 Chow
d500 Chow
d500 PBS
d500 ES-62
b
c
Chow
PBS
ES-62
Days
d
e
f
g
h
i
j
k
l
m
n
d56
Chow
PBS
ES-62
d340
Male
Female
Actinobacteria
Bacteroidetes
Firmicutes
Proteobacteria
Verrucomicrobia
o
p
q
r
Male Chow
Male PBS
Male ES-62
Female Chow
Female PBS
Female ES-62

Figure 10. Mathematical modelling of predictors of HCD feeding and targets of ES-62 in promoting healthspan. As described in Methods, to identify the pathophysiological, metabolic and immunological variables most robustly associated with ES-62 treatment, sex, and diet, each of the associated mouse cohorts was treated as classes in supervised machine learning classification. The top predictors of (a) HCD-feeding, (b) gender-biased effects of HFD-feeding (both achieving an average >95% accuracy of classification) and features most robustly indicative of ES-62-treatment of female (average 69.07% accuracy of classification; c) and male (average 54.47% accuracy of classification; d) HCD-fed mice are shown. Each bar represents the mean F score of the corresponding feature, horizontal black lines represent standard errors of the mean, the vertical dotted red line is the global mean F score of all features, and the shaded area is ≤ 1 standard error of the global F score mean. Features considered robustly associated with treatment are those that exceed the shaded area.

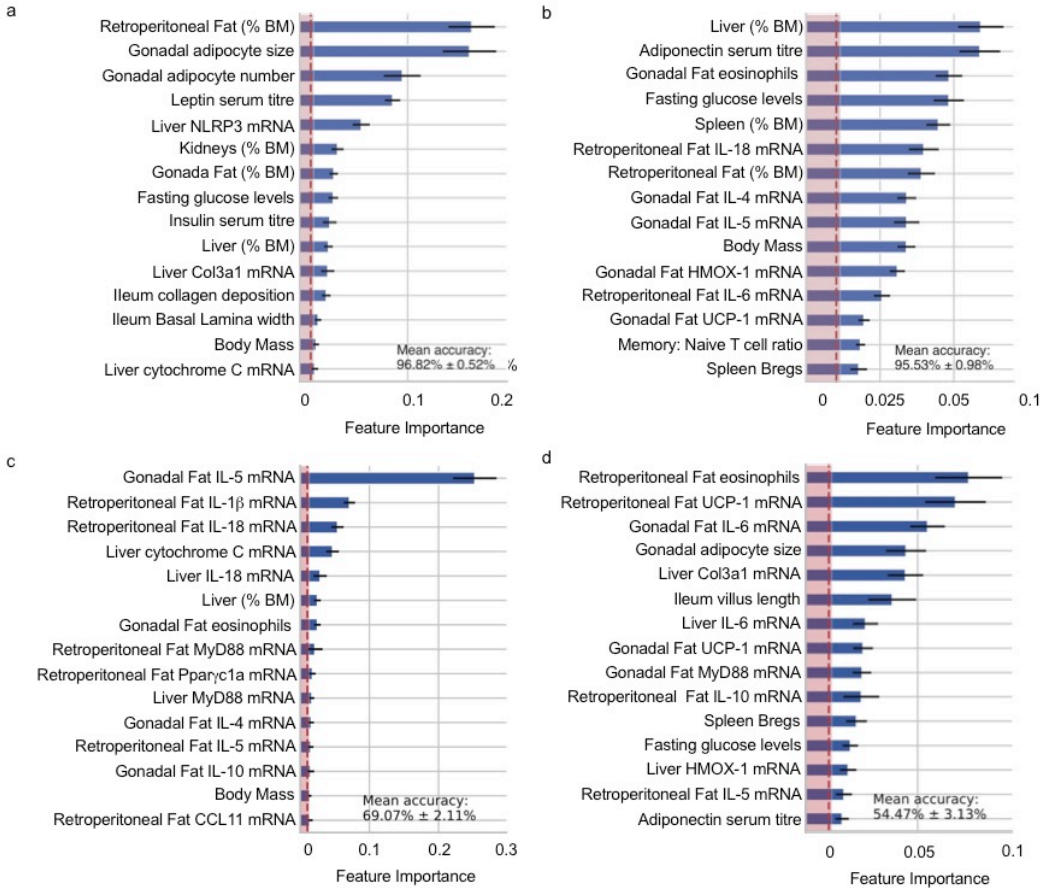
a
Retroperitoneal Fat (% BM)
Gonadal adipocyte size
Gonadal adipocyte number
Leptin serum titre
Liver NLRP3 mRNA
Kidneys (% BM)
Gonada Fat (% BM)
Fasting glucose levels
Insulin serum titre
Liver (% BM)
Liver Col3a1 mRNA
Ileum collagen deposition
Ileum Basal Lamina width
Body Mass
Liver cytochrome C mRNA
Mean accuracy:
96.82% ± 0.52%
0
0.1
0.2
Feature Importance
b
Liver (% BM)
Adiponectin serum titre
Gonadal Fat eosinophils
Fasting glucose levels
Spleen (% BM)
Retroperitoneal Fat IL-18 mRNA
Retroperitoneal Fat (% BM)
Gonadal Fat IL-4 mRNA
Gonadal Fat IL-5 mRNA
Body Mass
Gonadal Fat HMOX-1 mRNA
Retroperitoneal Fat IL-6 mRNA
Gonadal Fat UCP-1 mRNA
Memory: Naive T cell ratio
Spleen Bregs
Mean accuracy:
95.53% ± 0.98%
0
0.025
0.05
0.1
Feature Importance
c
Gonadal Fat IL-5 mRNA
Retroperitoneal Fat IL-1β mRNA
Retroperitoneal Fat IL-18 mRNA
Liver cytochrome C mRNA
Liver IL-18 mRNA
Liver (% BM)
Gonadal Fat eosinophils
Retroperitoneal Fat MyD88 mRNA
Retroperitoneal Fat Pparγc1a mRNA
Liver MyD88 mRNA
Gonadal Fat IL-4 mRNA
Retroperitoneal Fat IL-5 mRNA
Gonadal Fat IL-10 mRNA
Body Mass
Retroperitoneal Fat CCL11 mRNA
Mean accuracy:
69.07% ± 2.11%
0
0.1
0.2
0.3
Feature Importance
d
Retroperitoneal Fat eosinophils
Retroperitoneal Fat UCP-1 mRNA
Gonadal Fat IL-6 mRNA
Gonadal adipocyte size
Liver Col3a1 mRNA
Ileum villus length
Liver IL-6 mRNA
Gonadal Fat UCP-1 mRNA
Gonadal Fat MyD88 mRNA
Retroperitoneal Fat IL-10 mRNA
Spleen Bregs
Fasting glucose levels
Liver HMOX-1 mRNA
Retroperitoneal Fat IL-5 mRNA
Adiponectin serum titre
Mean accuracy:
54.47% ± 3.13%
0
0.05
0.1
Feature Importance

Supplementary Table 1 Descriptive statistics of longevity study

Sex	Treatment	Median	Mean	Min-Max	Oldest 10%	n
Male	PBS	629	636 ± 26.7	222-869	782	24
	ES-62	703	676 ± 29.8	193-869	821	24
Female	PBS	653	637 ± 16.7	443 -760	727	24
	ES-62	629	610 ± 23.9	366 -779	745	24

Supplementary Table 2 Incidence of pathology in longevity cohorts (numbers)

Pathology	Male		Female	
	PBS	ES-62	PBS	ES-62
GI tract obstruction/tumour	1	1	2	1
Hepatic tumour	11	10	10	10
Gonadal tumour	-	-	2	-
Multi-organ tumour	1	-	-	1
Musculoskeletal pathology	-	-	1	2
Non-healing dermatitis	-	-	1	-
>10% BM decline	18	21	21	17
Infection	-	-	-	1
Unknown	10	14	10	17
Number	24	24	24	24

Supplementary Table 3 Incidence of pathology in longevity cohorts (%)

Pathology	Male		Female	
	PBS	ES-62	PBS	ES-62
GI tract obstruction/tumour	4.2	4.2	8.3	4.2
Hepatic tumour	45.8	41.6	41.6	41.6
Gonadal tumour	-	-	8.3	-
Multi-organ tumour	4.2	-	-	4.2
Musculoskeletal pathology	-	-	4.2	8.3
Non-healing dermatitis	-	-	4.2	-
>10% BM decline	75	87.5	87.5	70.8
Infection	-	-	-	4.2
Unknown	41.6	58.3	41.6	37.5
Number	24	24	24	24

Supplementary Figure 1 Correlative analysis of BM and grip strength features with longevity. Correlation of age of death of male (a, c, e, g, i, k, m, o) and female (b, d, f, h, j, l, n, p) HCD- (PBS- and ES-62-tretaed) mice with (a, b) change in body mass over lifetime; (c, d) peak BM achieved; (e, f) BM at death; (g, h) BM at d116; (i, j) BM at d160; (k, l) BM at d340; (m, n) BM at d500; (o, p) decline in GF from peak strength.

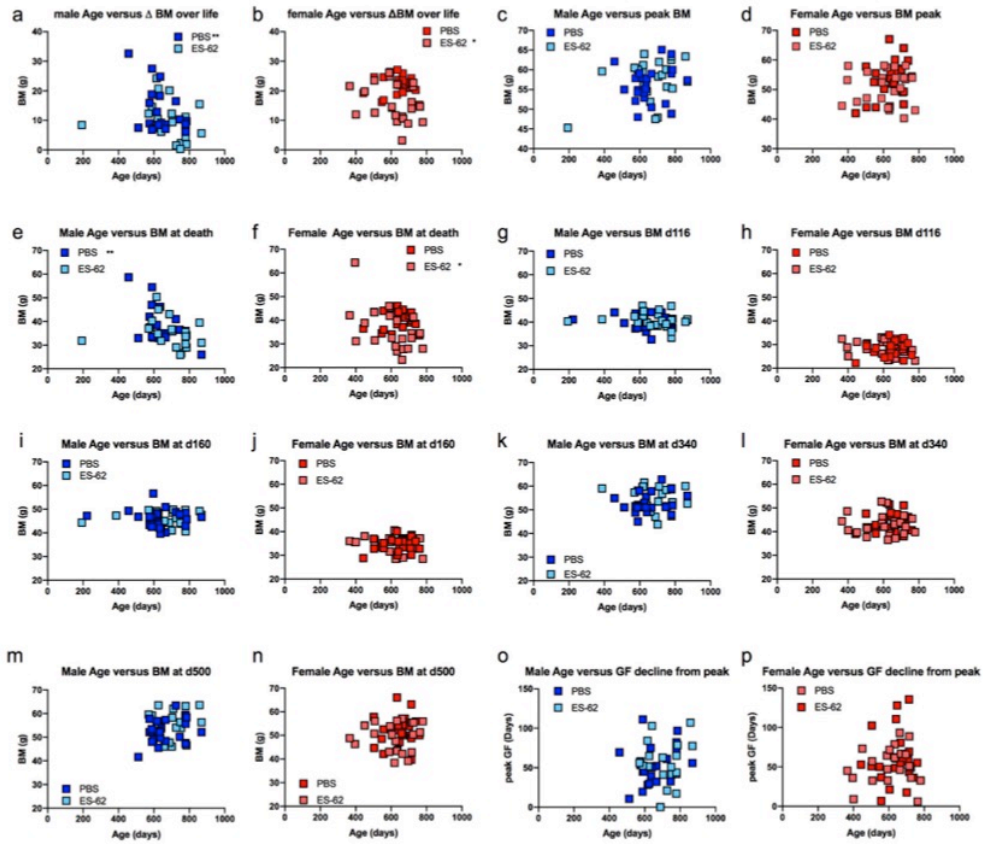

Supplementary Figure 2 Comparison of BM profiles of longevity and cross-sectional cohorts. Longitudinal analysis of BM measurements of the individual male (a, c, e, g) and female (b, d, f, h) HCD-fed mice in the survival and indicated cross-sectional cohorts where data are presented as mean values ± SEM of the mice surviving or culled at the indicated timepoints.

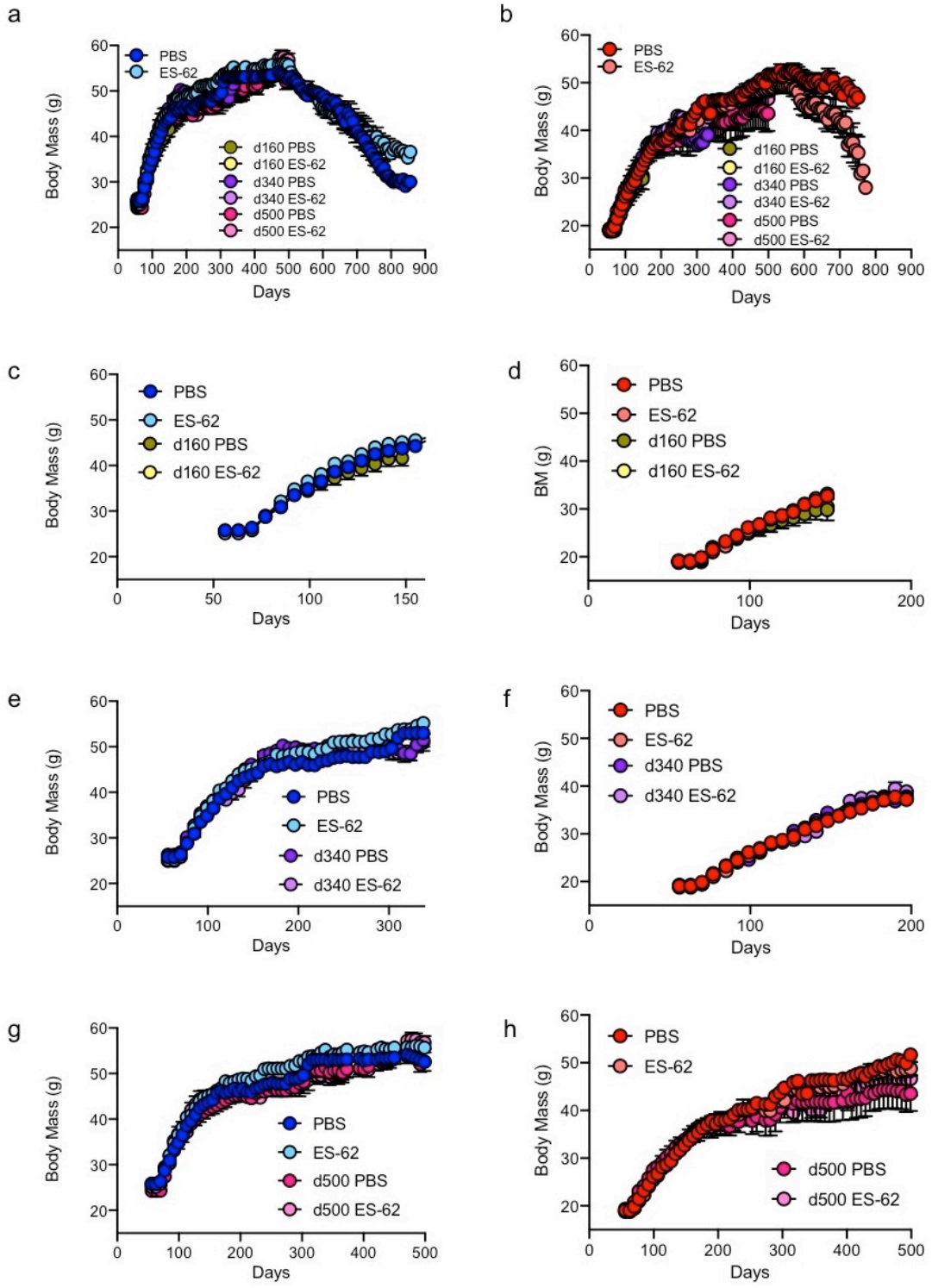

Supplementary Figure 3. HCD-induced adipocyte hypertrophy is not accompanied by hyperplasia. Quantitative analysis of adipocyte number/FOV in representative images of gonadal (a, b) and retroperitoneal (c, d) adipose tissue sections where data are presented as the mean values ± SEM where n=4-5 individual male (a, c) and female (b, d) chow- and HCD- (PBS- and ES-62-treated) mice at each time point and the values for each mouse were means derived from n=3 replicate analyses.

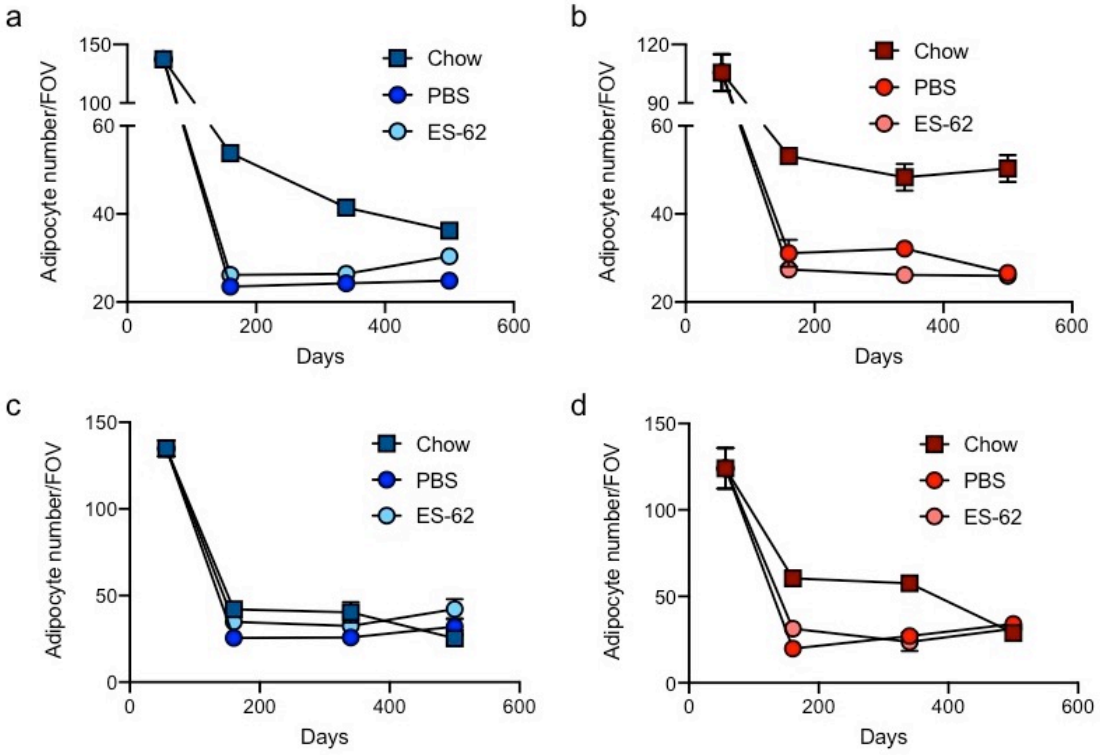

Supplementary Figure 4 Dysfunctional liver mitochondrial respiration in HCD-aged mice. Mitochondrial respiration (oxygen consumption rate, OCR) was measured in livers from male (a, c) and female (b, d) chow- or HFD (PBS or ES-62-treated) mice at cull at d340 and d500. Data are presented as the values ± SEM of individual mice where cohort sizes were: male, d340 - chow n=6, HFD-PBS n=7, HFD-ES-62, n=8; d500 chow - n=4, HFD-PBS n=4 HFD-ES-62, n=4; female, d340 - chow n=6; HFD-PBS n=11; HFD-ES-62 n=12; d500 - chow n=3, HFD-PBS n=4 HFD-ES-62, n=4.

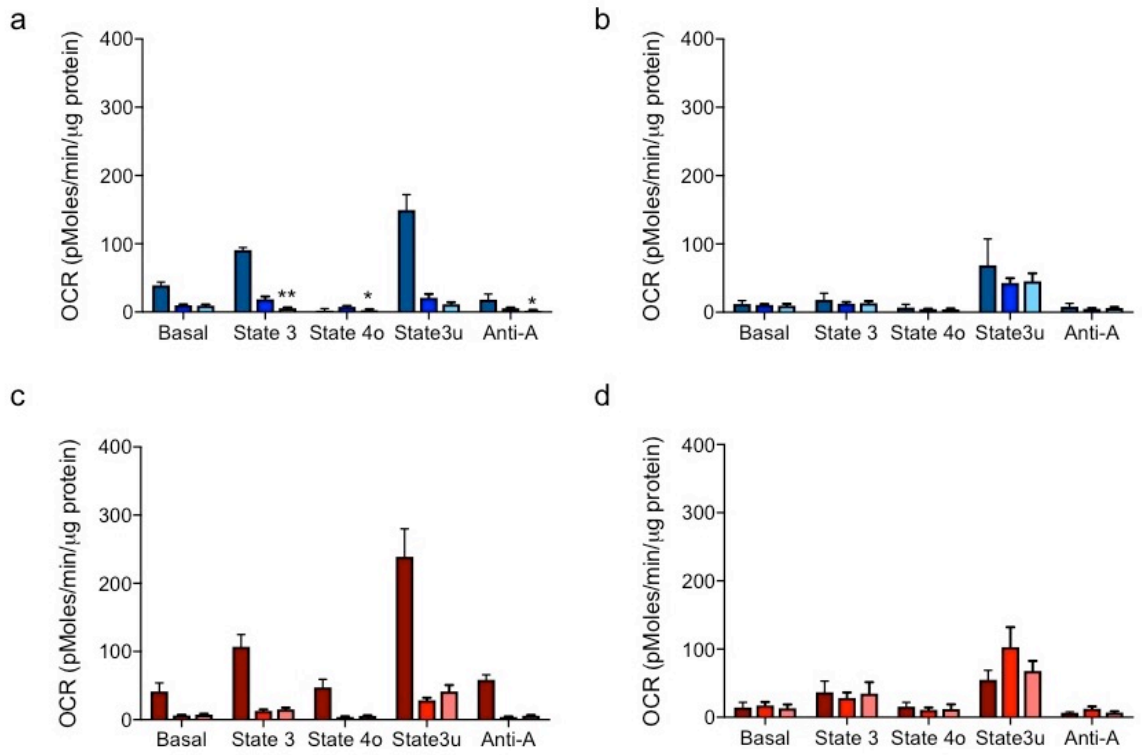

Supplementary Figure 5 Parameters of gut pathology in HCD-fed mice. Images of ileum and colon tissue from male and female chow- and HFD- (PBS- or ES-62-treated) mice were stained with H & E (to visualise basal lamina) and Gömöri's Trichrome (to visualise collagen deposition) and quantitative analysis of basal lamina width (ileum, a, b; colon, e, f) and collagen deposition (ileum, c, d; colon, g, h) are shown. Data are presented as the mean values ± SEM where n=4-6 individual male (a, c, e, g) and female (b, d, f, h) mice from each group at each time point and the values for each mouse are means derived from n=3 replicate analyses.

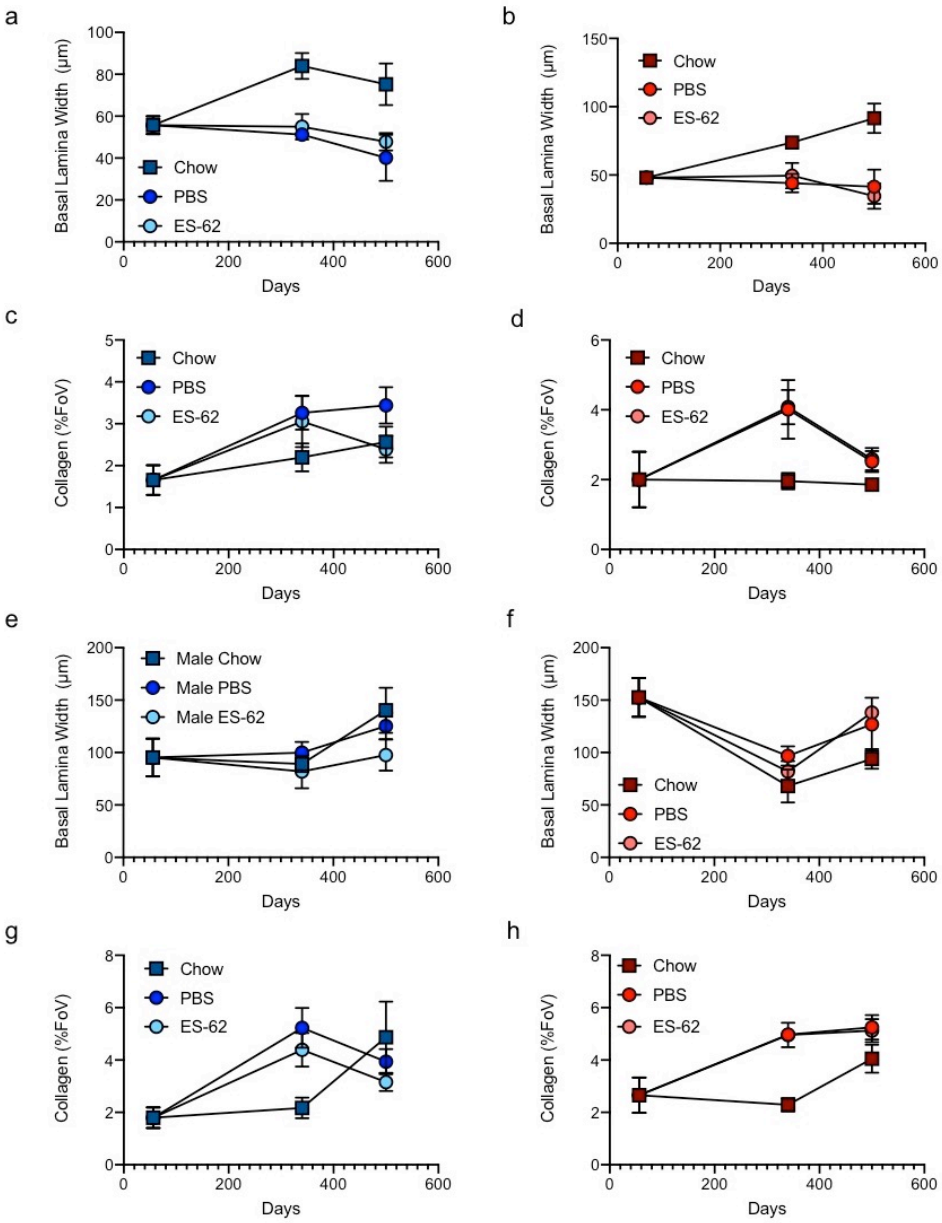

References

1 Fontana, L. & Partridge, L. Promoting health and longevity through diet: from model organisms to humans. *Cell* **161**, 106-118, doi:10.1016/ j.cell.2015.02.020 (2015).

2 Bennett, P. H., Magliano, D. J., Alberti, K. G. & Zimmet, P. Liberating non-communicable disease data. *Lancet Diabetes Endocrinol* **4**, 815-816, doi:10.1016/S2213-8587(16)30220-0 (2016).

3 Lopez-Otin, C., Blasco, M. A., Partridge, L., Serrano, M. & Kroemer, G. The hallmarks of aging. *Cell* **153**, 1194-1217, doi:10.1016/j.cell.2013.05.039 (2013).

4 Lee, Y. S., Wollam, J. & Olefsky, J. M. An Integrated View of Immunometabolism. *Cell* **172**, 22-40, doi:10.1016/j.cell.2017.12.025 (2018).

5 Hotamisligil, G. S. Inflammation, metaflammation and immunometabolic disorders. *Nature* **542**, 177-185, doi:10.1038/nature21363 (2017).

6 Hotamisligil, G. S. Foundations of Immunometabolism and Implications for Metabolic Health and Disease. *Immunity* **47**, 406-420, doi:10.1016/ j.immuni.2017.08.009 (2017).

7 Miller, R. A. Cell stress and aging: new emphasis on multiplex resistance mechanisms. *The Journals of Gerontology. Series A, Biological sciences and medical sciences* **64**, 179-182, doi:10.1093/gerona/gln072 (2009).

8 Collaborators, G. B. D. O. *et al.* Health Effects of Overweight and Obesity in 195 Countries over 25 Years. *N Engl J Med* **377**, 13-27, doi:10.1056/ NEJMoa1614362 (2017).

9 Harnett, M. M. & Harnett, W. Can Parasitic Worms Cure the Modern World's Ills? *Trends in Parasitology* **33**, 694-705, doi:10.1016/j.pt.2017.05.007 (2017).

10 Harnett, W. Secretory products of helminth parasites as immunomodulators. *Molecular and Biochemical Parasitology* **195**, 130-136, doi:10.1016/ j.molbiopara.2014.03.007 (2014).

11 Prescott, S. L. Early-life environmental determinants of allergic diseases and the wider pandemic of inflammatory noncommunicable diseases. *The Journal of Allergy and Clinical Immunology* **131**, 23-30, doi:10.1016/j.jaci.2012.11.019 (2013).

12 Helmby, H. Human helminth therapy to treat inflammatory disorders- where do we stand? *BMC Immunology* **16**, 12, doi:10.1186/s12865-015-0074-3 (2015).

13 Elliott, D. E. & Weinstock, J. V. Nematodes and human therapeutic trials for inflammatory disease. *Parasite Immunology* **39**, doi:10.1111/pim.12407 (2017).

14 Rodgers, D. T. *et al.* The Parasitic Worm Product ES-62 Targets Myeloid Differentiation Factor 88-Dependent Effector Mechanisms to Suppress Antinuclear Antibody Production and Proteinuria in MRL/lpr Mice. *Arthritis Rheumatol* **67**, 1023-1035, doi:10.1002/art.39004 (2015).

15 Coltherd, J. C. *et al.* The parasitic worm-derived immunomodulator, ES-62 and its drug-like small molecule analogues exhibit therapeutic potential in a model of chronic asthma. *Scientific Reports* **6**, 19224, doi:10.1038/srep19224 (2016).

16 Doonan, J. *et al.* The parasitic worm product ES-62 normalises the gut microbiota bone marrow axis in inflammatory arthritis. *Nature Communications* **10**, 1554, doi:10.1038/s41467-019-09361-0 (2019).

17 Jin, C., Henao-Mejia, J. & Flavell, R. A. Innate immune receptors: key regulators of metabolic disease progression. *Cell Metab* **17**, 873-882, doi:10.1016/j.cmet.2013.05.011 (2013).

18 Jialal, I., Kaur, H. & Devaraj, S. Toll-like receptor status in obesity and metabolic syndrome: a translational perspective. *J Clin Endocrinol Metab* **99**, 39-48, doi:10.1210/jc.2013-3092 (2014).

19 Bach, J. F. The hygiene hypothesis in autoimmunity: the role of pathogens and commensals. *Nature Reviews Immunology* **18**, 105-120, doi:10.1038/nri.2017.111 (2018).

20 Christ, A. *et al.* Western Diet Triggers NLRP3-Dependent Innate Immune Reprogramming. *Cell* **172**, 162-175 e114, doi:10.1016/j.cell.2017.12.013 (2018).

21 Griffin, C. *et al.* TLR4, TRIF, and MyD88 are essential for myelopoiesis and CD11c(+) adipose tissue macrophage production in obese mice. *The Journal of Biological Chemistry* **293**, 8775-8786, doi:10.1074/jbc.RA117.001526 (2018).

22 He, W. *et al.* Ageing potentiates diet-induced glucose intolerance, beta-cell failure and tissue inflammation through TLR4. *Scientific Reports* **8**, 2767, doi:10.1038/s41598-018-20909-w (2018).

23 Marais, G. A. B. *et al.* Sex gap in aging and longevity: can sex chromosomes play a role? *Biol Sex Differ* **9**, 33, doi:10.1186/s13293-018-0181-y (2018).

24 Gubbels Bupp, M. R., Potluri, T., Fink, A. L. & Klein, S. L. The Confluence of Sex Hormones and Aging on Immunity. *Frontiers in Immunology* **9**, 1269, doi:10.3389/fimmu.2018.01269 (2018).

25 Tower, J. Sex-Specific Gene Expression and Life Span Regulation. *Trends Endocrinol Metab* **28**, 735-747, doi:10.1016/j.tem.2017.07.002 (2017).

26 Miller, R. A., Harper, J. M., Galecki, A. & Burke, D. T. Big mice die young: early life body weight predicts longevity in genetically heterogeneous mice. *Aging Cell* **1**, 22-29 (2002).

27 Liew, C. W. *et al.* Ablation of TRIP-Br2, a regulator of fat lipolysis, thermogenesis and oxidative metabolism, prevents diet-induced obesity and insulin resistance. *Nature Medicine* **19**, 217-226, doi:10.1038/nm.3056 (2013).

28 Wu, D. *et al.* Eosinophils sustain adipose alternatively activated macrophages associated with glucose homeostasis. *Science (New York, N.Y* **332**, 243-247, doi:10.1126/science.1201475 (2011).

29 Molofsky, A. B. *et al.* Innate lymphoid type 2 cells sustain visceral adipose tissue eosinophils and alternatively activated macrophages. *The Journal of Experimental Medicine* **210**, 535-549, doi:10.1084/jem.20121964 (2013).

30 Kraakman, M. J., Murphy, A. J., Jandeleit-Dahm, K. & Kammoun, H. L. Macrophage polarization in obesity and type 2 diabetes: weighing down our understanding of macrophage function? *Frontiers in Immunology* **5**, 470, doi:10.3389/fimmu.2014.00470 (2014).

31 Boutens, L. & Stienstra, R. Adipose tissue macrophages: going off track during obesity. *Diabetologia* **59**, 879-894, doi:10.1007/s00125-016-3904-9 (2016).

32 Kumamoto, Y. *et al.* CD301b(+) Mononuclear Phagocytes Maintain Positive Energy Balance through Secretion of Resistin-like Molecule Alpha. *Immunity* **45**, 583-596, doi:10.1016/j.immuni.2016.08.002 (2016).

33 Wentworth, J. M. *et al.* Pro-inflammatory CD11c+CD206+ adipose tissue macrophages are associated with insulin resistance in human obesity. *Diabetes* **59**, 1648-1656, doi:10.2337/db09-0287 (2010).

34 Serbulea, V. *et al.* Macrophage phenotype and bioenergetics are controlled by oxidized phospholipids identified in lean and obese adipose tissue. *Proceedings of the National Academy of Sciences of the United States of America* **115**, E6254-E6263, doi:10.1073/pnas.1800544115 (2018).

35 Gomez-Hernandez, A., Beneit, N., Diaz-Castroverde, S. & Escribano, O. Differential Role of Adipose Tissues in Obesity and Related Metabolic and Vascular Complications. *Int J Endocrinol* **2016**, 1216783, doi:10.1155/2016/1216783 (2016).

36 Kowalski, G. M., Kraakman, M. J., Mason, S. A., Murphy, A. J. & Bruce, C. R. Resolution of glucose intolerance in long-term high-fat, high-sucrose-fed mice. *J Endocrinol* **233**, 269-279, doi:10.1530/JOE-17-0004 (2017).

37 van der Heijden, R. A. *et al.* High-fat diet induced obesity primes inflammation in adipose tissue prior to liver in C57BL/6j mice. *Aging* **7**, 256-268, doi:10.18632/aging.100738 (2015).

38 O'Toole, J. F., Patel, H. V., Naples, C. J., Fujioka, H. & Hoppel, C. L. Decreased cytochrome c mediates an age-related decline of oxidative phosphorylation in rat kidney mitochondria. *The Biochemical Journal* **427**, 105-112, doi:10.1042/BJ20091373 (2010).

39 Sheedfar, F., Di Biase, S., Koonen, D. & Vinciguerra, M. Liver diseases and aging: friends or foes? *Aging Cell* **12**, 950-954, doi:10.1111/acel.12128 (2013).

40 Lam, Y. Y. *et al.* Role of the gut in visceral fat inflammation and metabolic disorders. *Obesity (Silver Spring)* **19**, 2113-2120, doi:10.1038/oby.2011.68 (2011).

41 Rastelli, M., Knauf, C. & Cani, P. D. Gut Microbes and Health: A Focus on the Mechanisms Linking Microbes, Obesity, and Related Disorders. *Obesity (Silver Spring)* **26**, 792-800, doi:10.1002/oby.22175 (2018).

42 Heintz, C. & Mair, W. You are what you host: microbiome modulation of the aging process. *Cell* **156**, 408-411, doi:10.1016/j.cell.2014.01.025 (2014).

43 Vaiserman, A. M., Koliada, A. K. & Marotta, F. Gut microbiota: A player in aging and a target for anti-aging intervention. *Ageing Res Rev* **35**, 36-45, doi:10.1016/j.arr.2017.01.001 (2017).

44 Rera, M., Azizi, M. J. & Walker, D. W. Organ-specific mediation of lifespan extension: more than a gut feeling? *Ageing Res Rev* **12**, 436-444, doi:10.1016/j.arr.2012.05.003 (2013).

45 Rera, M., Clark, R. I. & Walker, D. W. Why do old flies die? *Aging* **5**, 586-587, doi:10.18632/aging.100589 (2013).

46 Regan, J. C. *et al.* Sex difference in pathology of the ageing gut mediates the greater response of female lifespan to dietary restriction. *eLife* **5**, e10956, doi:10.7554/eLife.10956 (2016).

47 Erben, U. *et al.* A guide to histomorphological evaluation of intestinal inflammation in mouse models. *Int J Clin Exp Pathol* **7**, 4557-4576 (2014).

48 Gallois, M., Gidenne, T., Fortun-Lamothe, L., Le Huerou-Luron, I. & Lalles, J. P. An early stimulation of solid feed intake slightly influences the morphological gut maturation in the rabbit. *Reprod Nutr Dev* **45**, 109-122 (2005).

49 Naradikian, M. S., Hao, Y. & Cancro, M. P. Age-associated B cells: key mediators of both protective and autoreactive humoral responses. *Immunological Reviews* **269**, 118-129, doi:10.1111/imr.12380 (2016).

50 Phalke, S. & Marrack, P. Age (autoimmunity) associated B cells (ABCs) and their relatives. *Current Opinion in Immunology* **55**, 75-80, doi:10.1016/j.coi.2018.09.007 (2018).

51 Riley, R. L., Khomtchouk, K. & Blomberg, B. B. Age-associated B cells (ABC) inhibit B lymphopoiesis and alter antibody repertoires in old age. *Cellular Immunology* **321**, 61-67, doi:10.1016/j.cellimm.2017.04.008 (2017).

52 Rosser, E. C. & Mauri, C. Regulatory B cells: origin, phenotype, and function. *Immunity* **42**, 607-612, doi:10.1016/j.immuni.2015.04.005 (2015).

53 Rosser, E. C. *et al.* Regulatory B cells are induced by gut microbiota-driven interleukin-1beta and interleukin-6 production. *Nature Medicine* **20**, 1334-1339, doi:10.1038/nm.3680 (2014).

54 Shaikh, S. R., Haas, K. M., Beck, M. A. & Teague, H. The effects of diet-induced obesity on B cell function. *Clinical and Experimental Immunology* **179**, 90-99, doi:10.1111/cei.12444 (2015).

55 Clark, R. I. *et al.* Distinct Shifts in Microbiota Composition during Drosophila Aging Impair Intestinal Function and Drive Mortality. *Cell Reports* **12**, 1656-1667, doi:10.1016/j.celrep.2015.08.004 (2015).

56 Cheng, J., Palva, A. M., de Vos, W. M. & Satokari, R. Contribution of the intestinal microbiota to human health: from birth to 100 years of age. *Current Topics in Microbiology and Immunology* **358**, 323-346, doi:10.1007/82_2011_189 (2013).

57 Hiippala, K. *et al.* The Potential of Gut Commensals in Reinforcing Intestinal Barrier Function and Alleviating Inflammation. *Nutrients* **10**, doi:10.3390/nu10080988 (2018).

58 Fujio-Vejar, S. *et al.* The Gut Microbiota of Healthy Chilean Subjects Reveals a High Abundance of the Phylum Verrucomicrobia. *Frontiers in Microbiology* **8**, 1221, doi:10.3389/fmicb.2017.01221 (2017).

59 Elderman, M., de Vos, P. & Faas, M. Role of Microbiota in Sexually Dimorphic Immunity. *Frontiers in Immunology* **9**, 1018, doi:10.3389/fimmu.2018.01018 (2018).

60 Vemuri, R. *et al.* The microgenderome revealed: sex differences in bidirectional interactions between the microbiota, hormones, immunity and disease susceptibility. *Semin Immunopathol* **41**, 265-275, doi:10.1007/s00281-018-0716-7 (2019).

61 Mariat, D. *et al.* The Firmicutes/Bacteroidetes ratio of the human microbiota changes with age. *BMC Microbiol* **9**, 123, doi:10.1186/1471-2180-9-123 (2009).

62 Flurkey, K., Currer, J. M. & Harrison, D. E. in *American College of Laboratory Animal Medicine* (ed James G Fox et al.) pp. 637-672 (Elsevier, Burlington, MA, 2007).

63 Dutta, S. & Sengupta, P. Men and mice: Relating their ages. *Life Sci* **152**, 244-248, doi:10.1016/j.lfs.2015.10.025 (2016).

64 Zhang, C. *et al.* Structural modulation of gut microbiota in life-long calorie-restricted mice. *Nature Communications* **4**, 2163, doi:10.1038/ncomms3163 (2013).

65 McInnes, I. B. *et al.* A novel therapeutic approach targeting articular inflammation using the filarial nematode-derived phosphorylcholine-containing glycoprotein ES-62. *J Immunol* **171**, 2127-2133 (2003).

66 Selman, C. *et al.* Evidence for lifespan extension and delayed age-related biomarkers in insulin receptor substrate 1 null mice. *Faseb J* **22**, 807-818, doi:10.1096/fj.07-9261com (2008).

67 Selman, C. *et al.* Ribosomal protein S6 kinase 1 signaling regulates mammalian life span. *Science (New York, N.Y* **326**, 140-144, doi:10.1126/science.1177221 (2009).

68 Cohen, C. A., Shea, A. A., Heffron, C. L., Schmelz, E. M. & Roberts, P. C. Intra-abdominal fat depots represent distinct immunomodulatory microenvironments: a murine model. *PLoS ONE* **8**, e66477, doi:10.1371/journal.pone.0066477 (2013).

69 Chusyd, D. E., Wang, D., Huffman, D. M. & Nagy, T. R. Relationships between Rodent White Adipose Fat Pads and Human White Adipose Fat Depots. *Front Nutr* **3**, 10, doi:10.3389/fnut.2016.00010 (2016).

70 Matthews, D. R. *et al.* Homeostasis model assessment: insulin resistance and beta-cell function from fasting plasma glucose and insulin concentrations in man. *Diabetologia* **28**, 412-419 (1985).

71 Mulvey, L., Sands, W. A., Salin, K., Carr, A. E. & Selman, C. Disentangling the effect of dietary restriction on mitochondrial function using recombinant inbred mice. *Mol Cell Endocrinol* **455**, 41-53, doi:10.1016/j.mce.2016.09.001 (2017).

72 Brand, M. D. & Nicholls, D. G. Assessing mitochondrial dysfunction in cells. *The Biochemical journal* **435**, 297-312, doi:10.1042/BJ20110162 (2011).

73 Pedregosa, F. *et al.* Scikit-learn: Machine Learning in Python. *Journal of Machine Learning Research* **12**, 2825-2830 (2011).

74 Waskom, M. *et al.* mwaskom/seaborn: v0.9.0 (July 2018). *Zenodo*, doi:http://doi.org/10.5281/zenodo.1313201 (2018).